

Resonant-magnetic-perturbation-induced plasma transport in H-mode pedestals

J.D. Callen,^{1, a)} A.J. Cole,² and C.C. Hegna¹

¹⁾ *University of Wisconsin, 1500 Engineering Drive, Madison, WI 53706-1609*

²⁾ *Columbia University, 201 S.W. Mudd, New York, NY 10027*

(Dated: 6 September 2012)

Plasma toroidal rotation reduces reconnection of externally applied resonant magnetic perturbation (RMP) fields $\delta\mathbf{B}$ on rational ($q = m/n$) magnetic flux surfaces. Hence, it causes radial perturbations $\delta B_{\rho m/n}$ to be small there, and thus inhibits magnetic island formation and stochasticity in the edge of high (H-) mode confinement tokamak plasmas. However, electron collisional damping combined with the spatial magnetic flutter $\delta B_{\rho m/n}$ induced by RMPs in the vicinity of rational surfaces causes a radial electron heat diffusivity $\chi_e^{RMP} \sim (1/2) \sum_{m,n} [\delta \hat{B}_{\rho m/n}(x)/B_0]^2 \chi_{e\parallel}^{\text{eff}}(x)$ in which $\chi_{e\parallel}^{\text{eff}} \sim (v_{Te}^2/\nu_e)/(1 + x^2/\delta_{\parallel}^2)$ is an effective parallel electron thermal diffusivity. These effects are reduced by magnetic shear effects at a distance x from rational surfaces for $|x| > \delta_{\parallel}$ but amplified for $\delta \hat{B}_{\rho m/n}(x) > \delta \hat{B}_{\rho m/n}(0)$. A kinetic, toroidal model of these RMP-flutter-induced plasma transport effects is developed and compared to a previously developed cylindrical model. The RMP-induced increases in plasma transport can be large enough to reduce plasma gradients in H-mode pedestals. Thus, they may contribute to suppressing edge localized modes in tokamak plasmas.

PACS numbers: 52.55.Fa, 52.25.Fi, 52.55.Dy, 52.30.Ex, 52.55.xZ

I. INTRODUCTION

The desirable high (H-) modes of plasma confinement in toroidal magnetic systems have large plasma parameter gradients in their edge pedestals (outer few % of the plasma radius). The width of the edge steep gradient region usually increases in time until the ideal magneto-hydrodynamic (MHD) peeling-ballooning (P-B) instability criterion¹⁻⁴ is exceeded and an edge localized mode (ELM^{5,6}) is precipitated. ELMs abruptly and repetitively relax the edge plasma gradients and deposit undesirable intense pulses of hot plasma onto solid materials (e.g., divertor plates) outside the plasma confinement region. They are particularly problematic⁷ for projected high performance fusion plasmas in ITER.⁸

Pioneering experiments⁹⁻¹² in DIII-D have used edge resonant magnetic perturbations (RMPs) to suppress ELMs. The physics of how RMPs control ELMs is not presently understood. A working hypothesis¹¹ is that multiple RMPs produce overlapping magnetic islands in the edge that cause magnetic stochasticity and enhanced plasma transport there. The sensitivity of RMP effects^{11,12} to field line pitch resonances and the striated density deposition profiles on divertor plates are in qualitative agreement with this model. However, extended MHD calculations usually predict¹³⁻¹⁵ that extant edge plasma toroidal flows limit “penetration” of RMP fields and thereby cause the RMP-induced radial perturbations to be small on rational surfaces where $q = m/n$. Thus, toroidal flows inhibit magnetic reconnection, island formation and stochasticity, particularly near the pedestal top where P-B instability drives may be largest.¹¹

While toroidal plasma “flow screening” usually reduces

radial perturbations on rational surfaces, RMPs nonetheless induce radial (ρ) magnetic perturbations $\delta B_{\rho m/n}$ in the vicinity of rational surfaces and hence throughout the edge plasma. This RMP-induced spatial “magnetic flutter” causes radial plasma electron heat transport¹⁶ that is largest at rational surfaces. However, the radially-averaged flutter-induced transport is dominated by the “residual” level of transport between rational surfaces — see Figs. 2 and 3. This residual transport is large enough to reduce pedestal top plasma gradients and hence may stabilize P-B modes, thereby suppressing ELMs. Flutter-induced plasma transport¹⁶ does not require magnetic stochasticity to produce radial electron heat transport as the Rechester-Rosenbluth model¹⁷ does.

The physics involved in magnetic-flutter-induced plasma transport can be illustrated by considering the effects of collisions on electrons moving along radially fluttering magnetic field lines. To do so the total magnetic field $\mathbf{B} \equiv \mathbf{B}_0 + \delta\mathbf{B}$ will be assumed to be composed of an axisymmetric equilibrium \mathbf{B}_0 for which $\mathbf{B}_0 \cdot \nabla\rho = 0$ plus 3D perturbations $\delta\mathbf{B}$. Here, the radial coordinate is the toroidal-flux-based minor radius $\rho \equiv \sqrt{\psi_t/\pi B_{t0}}$.

The radial field line excursions induced by a small m/n sinusoidal radial magnetic perturbation $\nabla\rho \cdot \delta\mathbf{B} = \delta \hat{B}_{\rho m/n} \cos(m\theta - n\zeta)$ will be considered first. Here, θ and ζ are straight-field-line poloidal and toroidal angles. Along magnetic field lines $\zeta = q(\rho)\theta$. Near the m/n rational surface $q(\rho) \simeq m/n + xq'$ in which $x \simeq \rho - \rho_{m/n}$ is the radial distance off the rational surface. Thus, along field lines the radial perturbation can be written as $\nabla\rho \cdot \delta\mathbf{B} \simeq \delta \hat{B}_{\rho m/n} \cos[k_{\parallel}(x)\ell]$ in which $\ell \equiv R_0 q(\theta - \theta_0)$ is the distance along a field line from an initial θ_0 , $k_{\parallel}(x) \equiv -k_{\theta}x/L_S$, $k_{\theta} \equiv m/\rho$ and $L_S \equiv R_0 q/s$ is the magnetic shear length with shear parameter $s \equiv \rho q'/q$.

In terms of these variables the radial projection of the magnetic field line equation $d\mathbf{x}/d\ell = \mathbf{B}/B$ is $dx/d\ell \simeq (\delta \hat{B}_{\rho m/n}/B_0) \cos[k_{\parallel}(x)\ell]$. Integrating this field

^{a)} callen@engr.wisc.edu; <http://homepages.cae.wisc.edu/~callen>

line equation over ℓ yields for an initial radial distance $x_0 \gg x_c = (\delta\hat{B}_{\rho m/n} L_S / k_\theta B_0)^{1/2} \equiv W/4$ [i.e., outside the assumed thin magnetic island of width W the magnetically reconnected $\delta\hat{B}_{\rho m/n}(0)$ produces at this rational surface — see Appendix A]

$$x(\ell) \simeq x_0 + \frac{\delta\hat{B}_{\rho m/n}(x_0)}{B_0} \frac{\sin[k_\parallel(x_0)\ell]}{k_\parallel(x_0)}. \quad (1)$$

When $k_\parallel(x_0)\ell \ll 1$ the radial excursion of a field line is $\Delta x_B \simeq \ell(\delta\hat{B}_{\rho m/n}/B_0)$ while for $k_\parallel(x_0)\ell \gg 1$ the radial excursions are oscillatory with a maximum radial excursion of $\Delta x_B \sim [1/k_\parallel(x_0)](\delta\hat{B}_{\rho m/n}/B_0)$.

Neglecting drifts of electrons off flux surfaces, typical electrons just stream along magnetic field lines with an electron thermal speed $v_{Te} \equiv \sqrt{2T_e/m_e}$. However, the maximum $\Delta\ell$ for this reversible parallel streaming motion is limited by the electron collision length $\lambda_e \equiv v_{Te}/\nu_e$. Thus, the maximum radial excursions of collisional electrons induced by the radial flutter of field lines are $\Delta x \sim \lambda_e \delta\hat{B}_{\rho m/n}/B_0$ for $k_\parallel(x_0)\lambda_e < 1$ and $\Delta x \sim [1/k_\parallel(x_0)]\delta\hat{B}_{\rho m/n}/B_0$ for $k_\parallel(x_0)\lambda_e > 1$.

Flutter plasma transport induced by electron collisions at a damping rate ν_e can now be illustrated in terms of the phenomenological radial diffusivity $D \sim (\Delta x)^2/2\Delta t$ in which Δx is the radial step taken in a time $\Delta t \sim 1/\nu_e$:

$$D \sim \frac{v_{Te}^2}{2\nu_e} \left[\frac{\delta\hat{B}_{\rho m/n}(x_0)}{B_0} \right]^2 \quad \text{for } k_\parallel(x_0)\lambda_e < 1, \quad (2)$$

$$D \sim \frac{\nu_e}{2k_\parallel(x_0)^2} \left[\frac{\delta\hat{B}_{\rho m/n}(x_0)}{B_0} \right]^2 \quad \text{for } k_\parallel(x_0)\lambda_e > 1. \quad (3)$$

The kinetic analysis in Section III and Appendix A of this paper show that these results are obtained under the assumption that the effective ν_e is greater than both the plasma rotation frequency ω and the particle drift frequency ω_d . The apparent divergence in (2) as $\nu_e \rightarrow 0$ would be resolved by finite ω and/or ω_d effects.

The formula in (2) is applicable near (but outside any magnetic island that may be present at) the m/n rational surface. Its v_{Te}^2/ν_e coefficient is proportional to the usual Braginskii¹⁸ collisional parallel electron heat diffusivity $\chi_{e\parallel}$. Far away from a rational surface, magnetic shear reduces the effective parallel electron heat diffusivity and yields (3) which decreases as $1/k_\parallel(x_0)^2 \sim 1/x_0^2$. However, flow-screened radial magnetic perturbations $\delta\hat{B}_{\rho m/n}(x_0)$ typically^{13–15} grow approximately linearly with distance x_0 away from a rational surface. The spatial growth of $\delta\hat{B}_{\rho m/n}(x_0)^2$ away from rational surfaces tends to cancel the magnetic shear reduction effects to produce a significant residual electron diffusivity between rational surfaces.

Fluid and kinetic approaches based on analyzing and determining the parallel electron heat flows induced by $\delta\hat{B}_{\rho m/n}$ near the m/n rational surface can also be used to explore the physical processes involved in RMP-flutter-

induced transport — see Appendix A. This appendix discusses how electron collisions resolve the singular behavior of the parallel electron heat flux near a rational surface and cause $\mathbf{B} \cdot \nabla T_e \simeq \mathbf{B}_0 \cdot \nabla \delta T_e + \delta \mathbf{B} \cdot \nabla T_{e0}$ to be small but nonzero for $\nu_e \neq 0$ and large but finite $\chi_{e\parallel}$. In addition, this appendix shows that outside a m/n magnetic island the gradient of T_e is dominantly radial (i.e., $\nabla T_e \simeq \nabla \rho dT_{e0}/d\rho$). This is why the lowest order electron distribution is a Maxwellian $f_{Me}(\rho)$ in the kinetic analyses used in Ref. 19 and developed for toroidal geometry here and the “drive” for the RMP-induced kinetic response is proportional to $\delta\hat{B}_{\rho m/n} df_{Me}/d\rho$.

For the parameters typical of those near the pedestal top in DIII-D RMP experiments^{11,20} given in Appendix B, the Braginskii¹⁸ $\chi_{e\parallel} \sim 10^{10} \text{ m}^2 \text{ s}^{-1}$. Thus, very small RMP fields $\delta\hat{B}_{\rho m/n}/B_0 \gtrsim \sqrt{2} \times 10^{-5}$ could in principle produce radial electron diffusivities D that can exceed the typical radial electron thermal diffusivity levels $\chi_e \sim 1 \text{ m}^2 \text{ s}^{-1}$ in tokamak H-mode pedestals.²¹

A previous paper¹⁹ developed a model for the magnetic-flutter-induced plasma transport effects of RMPs in the plasma edge using a cylindrical screw-pinch magnetic field model and compared various model predictions with low collisionality pedestal data from DIII-D RMP experiments.¹¹ This paper develops a more physically relevant and complete kinetic-based, toroidal theory of these RMP-flutter-induced plasma transport effects. It uses a Lorentz collision model, accounts for parallel flows only being carried by untrapped particles, resolves a collisional boundary layer in velocity space and includes the finite aspect ratio effects of the toroidal geometry.

In developing models of RMP-flutter-induced plasma transport, the magnetic perturbations are not calculated self-consistently. Rather, it will be assumed that they are provided by linear extended MHD modeling codes^{13–15} that include the effects of flow-screening. Further, it will be assumed that flow-screening causes the radial perturbations to be small at rational surfaces. Thus, it will be assumed that any magnetic islands the RMPs produce have negligible width. Effects of finite width magnetic islands on T_e profiles²² are discussed in Section IV.

The body of this paper develops a kinetic-based, toroidal model of RMP-flutter-induced radial electron heat and density transport fluxes in the vicinity of rational surfaces in the pedestal region of tokamak H-mode plasmas. For comparison purposes, the next section (II) briefly summarizes the analogous results obtained previously¹⁹ using a cylindrical model. The following section (III) develops the more relevant kinetic-based, fully toroidal model of the parallel flows and radial plasma transport induced by RMPs. Section IV compares the results of the two models and discusses various other issues. The final section summarizes the results and implications of this toroidal model for RMP-induced effects on plasma transport, P-B stability and ELMs in H-mode pedestals of tokamak plasmas. Appendix A discusses how electron collisions produce the irreversibility needed for flutter model plasma transport and validity conditions

for the model. Appendix B presents typical parameters at the top of DIII-D pedestals in which RMPs suppress ELMs which are used throughout this paper in numerical evaluations of flutter model parameters.

II. CYLINDRICAL MODEL RESULTS

In the cylindrical (subscript c) model¹⁹ the in-phase component of the lowest order parallel electron flow $\delta V_{e\parallel c}$ and heat flux $\delta q_{e\parallel c}$ due to radial magnetic flutter $\delta B_{\rho m/n}$ induced by a single m/n RMP field component are

$$\begin{bmatrix} n_e \delta V_{e\parallel c} \\ \delta q_{e\parallel c} \end{bmatrix} = -n_e \frac{\delta B_{\rho m/n}(\mathbf{x}, t)}{B_0} \begin{bmatrix} D_{e\parallel}^{\text{eff}} d \ln \hat{p}_e / d\rho \\ \chi_{e\parallel}^{\text{eff}} dT_e / d\rho \end{bmatrix}. \quad (4)$$

Here, the thermodynamic force for the electron flow is a combination of the radial electron pressure gradient and radial electric field $E_\rho = -d\Phi_0/d\rho$:

$$\frac{d \ln \hat{p}_e}{dr} \equiv \frac{d \ln p_e}{d\rho} - \frac{e}{T_e} \frac{d\Phi_0}{d\rho} = \frac{d \ln p_e}{d\rho} + \frac{eE_\rho}{T_e}. \quad (5)$$

These results were obtained using an effective electron collision frequency ν_{eff} independent of the electron speed v . If the speed dependence of the collision frequency is kept, in general the right side of (4) is replaced by a matrix of diffusion coefficients driven by the thermodynamic forces — see (34) below.

A Padé-approximate effective parallel electron thermal diffusivity¹⁹ can be written in terms of the cylindrical model reference parallel electron thermal diffusivity $\chi_{\parallel c}^{\text{ref}}$ and a magnetic-shear-induced geometric factor $G_c(x)$:

$$\chi_{e\parallel}^{\text{eff}} \simeq \chi_{\parallel c}^{\text{ref}}(\rho) G_c(x), \quad \text{in which} \quad (6)$$

$$\chi_{\parallel c}^{\text{ref}}(\rho) \equiv c_{\nu T} \frac{v_{Te}^2}{\nu_{\text{eff}}} \simeq \frac{5}{4} \left(\frac{\langle n_u \rangle}{n_0} \right)^3 \frac{v_{Te}^2}{\nu_e}, \quad (7)$$

$$G_c(x) \equiv \frac{1}{1 + x^2 / \delta_{\parallel c}^2}. \quad (8)$$

Here, $x \simeq \rho - \rho_{m/n}$ is the radial distance off the rational surface where $q(\rho_{m/n}) = m/n$, which is defined more precisely in (27) below.

The analysis of Ref. 19 used an effective phenomenological electron collision frequency $\nu_{\text{eff}} \simeq \nu_e / (\langle n_u \rangle / n_0)^2$ in which $\langle n_u \rangle / n_0 \simeq 1 - (2/\pi) \sqrt{\Delta B / B_{\text{max}}}$ is the flux-surface-averaged (FSA) fraction of untrapped (u) particles. This form of ν_{eff} crudely models the important effect toroidal geometry has on collisions of untrapped particles that is not present in cylindrical plasmas but which will be derived in detail in the next section. Here, $\Delta B \equiv B_{\text{max}} - B_{\text{min}}$ in which B_{max} , B_{min} are the maximum, minimum of $|\mathbf{B}_0|$ on an axisymmetric flux surface. As indicated in the last form of (7), the coefficient $c_{\nu T} = (5/4) (\langle n_u \rangle / n_0)$ in this model.¹⁹ For the parameters in Appendix B, $B_{\text{max}}/B_{\text{min}} \simeq 2$, the inverse aspect ratio is $\epsilon \simeq 0.33$, $\langle n_u \rangle / n_0 \simeq 0.55$ and $\nu_{\text{eff}} \simeq 2 \times 10^5 \text{ s}^{-1}$.

The parallel density diffusivity $D_{e\parallel}^{\text{eff}}$ in (4) has the same form as (6) but with¹⁹ $c_{\nu T} \rightarrow c_{\nu n} = (1/2) (\langle n_u \rangle / n_0)$. If $\langle n_u \rangle / n_0$ is set to unity, the numerical factor of 5/4 in the reference parallel electron thermal diffusivity in (7) is close to the Braginskii¹⁸ collisional parallel electron thermal diffusivity for which $c_{\nu T} = 1.6$ for $Z_i = 1$.

The magnetic-shear-induced factor $G_c(x)$ causes $\chi_{e\parallel}^{\text{eff}}$ and $D_{e\parallel}^{\text{eff}}$ to decrease as $1/x^2$ for $|x| \gg \delta_{\parallel c}$. The parameter that characterizes the radial extent of the region over which magnetic flutter induces the largest parallel electron flows in this cylindrical model is¹⁹

$$\delta_{\parallel c} \equiv \frac{\sqrt{2} \nu_{\text{eff}} L_S}{k_\theta v_{Te}} = \sqrt{2} \left(\frac{n_0}{\langle n_u \rangle} \right)^2 \frac{L_S}{k_\theta \lambda_e}. \quad (9)$$

For the parameters given in Appendix B, $\delta_{\parallel c} \simeq 0.22 \text{ cm}$.

Radial electron density and heat fluxes induced by the m/n RMP-induced fluttering field are¹⁹

$$\begin{bmatrix} \delta \Gamma_{ec}^{m/n} \\ \delta \Upsilon_{ec}^{m/n} \end{bmatrix} \equiv \begin{bmatrix} n_e \delta V_{e\rho} \\ \delta q_{e\rho} \end{bmatrix} = -n_e \begin{bmatrix} D_{ec}^{m/n} d \ln \hat{p}_e / d\rho \\ \chi_{ec}^{m/n} dT_e / d\rho \end{bmatrix}. \quad (10)$$

Again, if the speed dependence of the collision frequency is kept, in general the right side of (10) is replaced by a matrix of diffusion coefficients driven by the thermodynamic forces — see (36) and (38) below.

The cylindrical model¹⁹ electron thermal diffusivity induced by a m/n radial field Fourier coefficient $\delta \hat{B}_{\rho m/n}$ can be written as

$$\chi_{ec}^{m/n} = \frac{\chi_{\parallel c}^{\text{ref}}(\rho)}{2} \left[\frac{\delta \hat{B}_{\rho m/n}(x)}{B_0} \right]^2 G_c(x). \quad (11)$$

The analogous magnetic-flutter-induced radial density diffusivity $D_{ec}^{m/n}$ has the same form but with $\chi_{e\parallel}^{\text{eff}} \rightarrow D_{e\parallel}^{\text{eff}}$ and hence $c_{\nu T} \rightarrow c_{\nu n}$; thus, $D_{ec}^{m/n} / \chi_{ec}^{m/n} = 2/5$. For the parameters in Appendix B, $\chi_{\parallel c}^{\text{ref}} \simeq 1.45 \times 10^9 \text{ m}^2 \text{ s}^{-1}$.

The radial electron thermal diffusivity in (11) needs to be evaluated using the radial magnetic perturbation profile $\delta \hat{B}_{\rho m/n}(\rho)$ in the plasma. Since the flow-screened magnetic perturbations are not being calculated self-consistently, a cylindrical model $\delta \hat{B}_{\rho m/n}$ profile, which is limited to $|x| < 1/k_\theta$, was used in Ref. 19:

$$\delta \hat{B}_{\rho m/n}^{\text{pl}}(x) = \delta \hat{B}_{\rho m/n}^{\text{vac}} \sqrt{1/f_{\text{scr}}^2 + k_\theta^2 x^2}. \quad (12)$$

Here, the pl superscript indicates the flow-screened value in the plasma, the vac superscript indicates the vacuum value and $f_{\text{scr}} \equiv \delta \hat{B}_{\rho m/n}^{\text{vac}} / \delta \hat{B}_{\rho m/n}^{\text{pl}}(0)$ is the “flow screening factor” — ratio of vacuum to flow-screened field on the rational surface. For this assumed flow screening function, at large distances from the rational surface the $1/x^2$ dependence of G_c cancels the $k_\theta^2 x^2$ dependence of $\delta \hat{B}_{\rho m/n}^{\text{pl}}(x)^2$ to produce $\chi_{m/n}^{\text{ref}} \equiv (1/2) [\delta \hat{B}_{\rho m/n}^{\text{vac}} / B_0]^2 \chi_{\parallel c}^{\text{ref}} (k_\theta \delta_{\parallel c})^2$, which yields $\chi_{m/n}^{\text{ref}} \simeq 0.086 \text{ m}^2 \text{ s}^{-1}$ for the parameters in Appendix B.

Since $1/k_\theta \sim 6.7$ cm and the spacing between rational surfaces is $1/nq' \simeq 2.8$ cm for the parameters in Appendix B, the RMP-induced responses from a number of m/n usually overlap. Thus, the total cylindrical model RMP-induced radial electron density and thermal diffusivities are obtained by summing over all the relevant m, n magnetic field components in the edge plasma:

$$\chi_{ec}^{\text{RMP}} \equiv \sum_{mn} \chi_{ec}^{m/n}, \quad D_{ec}^{\text{RMP}} \equiv \sum_{mn} D_{ec}^{m/n}. \quad (13)$$

III. KINETIC-BASED TOROIDAL MODEL

The details of the collisional kinetics and the tokamak magnetic field geometry cause modifications of the numerical coefficients and radial structure of $\chi_{ec}^{m/n}$. For the parameters in Appendix B, the electron collision length $\lambda_e \simeq 350$ m is long compared to the poloidal periodicity length along field lines of $2\pi R_0 q \simeq 37$ m. Thus, electron responses to RMP fields need to be averaged over the poloidal periodicity. Also, since $|\mathbf{B}_0|$ varies significantly over a flux surface ($\Delta B/B_{\min} \sim 1$), only circulating (untrapped) electrons contribute to the parallel flow $\delta V_{e\parallel}$ and heat flux $\delta q_{e\parallel}$. Further, a kinetic approach is needed because the parallel electron speed v_{\parallel} varies along a field line. Also, the effective circulating electron collision frequency ν_{eff} needs to be derived kinetically. Finally, because of the large inverse aspect ratio $\epsilon \simeq 0.33$ and nearness of the pedestal region to the magnetic separatrix, tokamak magnetic field geometry details are important.

The lowest order tokamak axisymmetric magnetic field will be written as $\mathbf{B}_0 \equiv \mathbf{B}_t + \mathbf{B}_p = I\nabla\zeta + \nabla\zeta \times \nabla\psi_p = \nabla\psi \times \nabla[q(\psi_p)\theta - \zeta]$ in which the toroidal, poloidal fields are $\mathbf{B}_t, \mathbf{B}_p, I(\psi_p) \equiv RB_t, R$ is the major radius, $2\pi\psi_p(\rho)$ is the poloidal flux and $q(\psi_p) \equiv \mathbf{B}_0 \cdot \nabla\zeta / \mathbf{B}_0 \cdot \nabla\theta = d\psi_t/d\psi_p = d\zeta/d\theta$. The (non-orthogonal) curvilinear coordinates that will be used are a toroidal-flux-based radial coordinate $\rho \equiv \sqrt{\psi_t/\pi B_{t0}}$, ‘‘straight-field-line’’ poloidal angle θ and axisymmetry toroidal angle ζ for which the Jacobian is $\sqrt{g} \equiv 1/\nabla\rho \cdot \nabla\theta \times \nabla\zeta = \psi_p'/\mathbf{B}_0 \cdot \nabla\theta = \psi_p'R^2q/I$ in which $\psi_p' \equiv d\psi_p/d\rho$. Here, $B_{t0} \equiv I(0)/R_0$ is the strength of the toroidal magnetic field at the magnetic axis where $R = R_0$. Taking the $\nabla\theta$ projection of the $d\mathbf{x}/d\ell = \mathbf{B}_0(\rho, \theta)/B_0(\rho, \theta)$ definition of a magnetic field line yields for the distance ℓ along \mathbf{B}_0 the differential equation $d\ell = d\theta B_0/\mathbf{B}_0 \cdot \nabla\theta$. The flux-surface-average (FSA) of a function $f(\mathbf{x})$ is

$$\langle f \rangle \equiv \frac{\int_{-\pi}^{\pi} d\zeta \int_{-\pi}^{\pi} d\theta \sqrt{g} f}{\int_{-\pi}^{\pi} d\zeta \int_{-\pi}^{\pi} d\theta \sqrt{g}} = \frac{\int_{-\pi}^{\pi} d\zeta \int_{-\pi}^{\pi} d\theta f / \mathbf{B}_0 \cdot \nabla\theta}{\int_{-\pi}^{\pi} d\zeta \int_{-\pi}^{\pi} d\theta / \mathbf{B}_0 \cdot \nabla\theta}. \quad (14)$$

A. Drift-kinetic equation and analysis of it

Neglecting gyromotion, electron guiding centers (subscript gc) just stream along a magnetic field line and drift slowly off of it: $\mathbf{v}_{\text{gc}} \equiv v_{\parallel}\mathbf{B}/B + \mathbf{v}_d = v_{\parallel}(\mathbf{B}_0 + \delta\mathbf{B})/B + \mathbf{v}_d$

in which $v_{\parallel} \equiv \mathbf{B} \cdot \mathbf{v}_{\text{gc}}/B$ and \mathbf{v}_d is a combination of the $\mathbf{E} \times \mathbf{B}$, gradient-B and curvature drifts. Thus, the drift-kinetic equation (DKE) for electrons becomes

$$\frac{\partial f_e}{\partial t} + \left[\frac{v_{\parallel}}{B} (\mathbf{B}_0 + \delta\mathbf{B}) + \mathbf{v}_d \right] \cdot \nabla f_e + \frac{d\varepsilon}{dt} \frac{\partial f_e}{\partial \varepsilon} = \mathcal{C}\{f_e\}. \quad (15)$$

Here, the electron ($q_e = -e$) guiding center energy is $\varepsilon \equiv m_e v^2/2 - e\Phi$ in which Φ is the electrostatic potential.

The magnetic perturbations $\delta\mathbf{B}$ will be ordered to be gyro-radius small: $|\delta\mathbf{B}|/B_0 \sim |\mathbf{v}_d|/v_{Te} \sim \varrho_e/L_{\perp} \ll 1$. In addition, the analysis will be restricted to field lines outside any possible magnetic island at the m/n rational surface so that field lines just flutter a small distance radially $\propto \delta\hat{B}_{\rho m/n}/B_0$ as indicated in (1). Thus, the lowest order equilibrium drift-kinetic equation obtained using $d\varepsilon/dt = 0$ and neglecting the gyro-radius-small $\delta\mathbf{B}$ and \mathbf{v}_d effects is $(v_{\parallel}/B_0) \mathbf{B}_0 \cdot \nabla f_{e0} = \mathcal{C}\{f_{e0}\}$. Its solution is a Maxwellian constant along \mathbf{B}_0 (i.e., the axisymmetric magnetic flux surfaces labeled by ρ):

$$f_{e0} = f_{Me}(\rho, \varepsilon) \equiv \frac{n_e(\rho) e^{-e\Phi_0(\rho)/T_e(\rho)}}{[2\pi T_e(\rho)/m_e]^{3/2}} e^{-\varepsilon/T_e(\rho)}, \quad (16)$$

in which the macroscopic radial variations of the electron density n_e and temperature T_e , and the lowest order potential Φ_0 are indicated explicitly.

Next, a perturbed DKE will be obtained for the perturbed electron distribution $\delta f_e \equiv f_e - f_{Me}$. A perturbed potential $\delta\Phi$ and toroidal inductive electric field \mathbf{E}^A will be allowed for in the initial, general analysis. Then, $d\delta\varepsilon/dt \equiv (\partial/\partial t + \mathbf{v}_{\text{gc}} \cdot \nabla) (-e\delta\Phi) - e\mathbf{v}_{\text{gc}} \cdot \mathbf{E}^A = -e[\partial\delta\Phi/\partial t + (v_{\parallel}/B_0)(\mathbf{B}_0 \cdot \nabla\delta\Phi) + \mathbf{v}_d \cdot \nabla\delta\Phi] - e\mathbf{v}_{\text{gc}} \cdot \mathbf{E}^A$. It will be convenient to write the perturbed DKE as an equation for the perturbed non-adiabatic distribution:

$$\delta h \equiv \delta f_e - (e/T_e) \delta\Phi(\mathbf{x}, t) f_{Me}. \quad (17)$$

Then, since when the collision operator acts on a Maxwellian distribution it vanishes, $\mathcal{C}\{\delta f_e\} = \mathcal{C}\{\delta h\}$ and hence the linearized perturbed DKE can be written as

$$\begin{aligned} & \frac{\partial \delta h}{\partial t} + \left[\frac{v_{\parallel}}{B_0} \mathbf{B}_0 + \mathbf{v}_d \right] \cdot \nabla \delta h - \mathcal{C}\{\delta h\} \\ & = -\frac{v_{\parallel}}{B_0} \delta\mathbf{B} \cdot \nabla f_{Me} - \mathbf{v}_d \cdot \nabla f_{Me} - \frac{e}{T_e} \mathbf{v}_{\text{gc}} \cdot \mathbf{E}^A f_{Me}. \end{aligned} \quad (18)$$

The last two terms on the right side of this equation will be omitted henceforth since they represent drives for neo-classical and fluctuation-induced (for $\hat{\mathbf{v}}_{\text{gc}} \simeq \hat{\mathbf{E}} \times \mathbf{B}/B^2$) transport processes and the toroidal voltage induced by the inductive electric field in the plasma that are not of interest here. The non-adiabatic response δh is caused by the magnetic flutter $\delta B_{\rho}(\mathbf{x}, t) \equiv \nabla\rho \cdot \delta\mathbf{B}$ of field lines radially across plasma profile gradients:

$$\delta\mathbf{B} \cdot \nabla f_{Me} \equiv (\delta\mathbf{B} \cdot \nabla\rho) \left[\frac{\partial f_{Me}}{\partial \rho} \right]_{\varepsilon} = \delta B_{\rho}(\mathbf{x}, t) f'_{Me}, \quad (19)$$

in which

$$f'_{Me} = f_{Me} \left[\frac{d \ln p_e}{d\rho} - \frac{e}{T_e} \frac{d\Phi_0}{d\rho} + \left(\frac{v^2}{v_{Te}^2} - \frac{5}{2} \right) \frac{d \ln T_e}{d\rho} \right]. \quad (20)$$

Here, the radial component of $\delta\mathbf{B}$ is really its contravariant ($\mathbf{e}^\rho \equiv \nabla\rho$) projection that would normally be labeled as $\delta B_{m/n}^\rho$. A subscript ρ is used here so this symbol is similar to that used in the cylindrical model.

For kinetic analysis of $\delta\mathbf{B}$ -induced effects near a $q = m/n$ rational surface, the most useful independent variables are local helical ones:^{23,24} ρ , θ and a Clebsch-type helical angle valid on all flux surfaces $\alpha \equiv \zeta - (m/n)\theta$. In terms of these variables the parallel derivative in (18) is $\mathbf{B}_0 \cdot \nabla \delta h = (\mathbf{B}_0 \cdot \nabla \theta) [\partial/\partial\theta + (q - m/n)(\partial/\partial\alpha)] \delta h$. The desired perturbed DKE in ρ, θ, α variables is thus

$$\begin{aligned} \frac{\partial \delta h}{\partial t} + \frac{v_{\parallel}}{B_0} (\mathbf{B}_0 \cdot \nabla \theta) \left[\frac{\partial \delta h}{\partial \theta} + (q - m/n) \frac{\partial \delta h}{\partial \alpha} \right] \\ + \mathbf{v}_d \cdot \nabla \delta h - \mathcal{C}\{\delta h\} = - \frac{v_{\parallel}}{B_0} \delta B_{\rho} f'_{Me}. \end{aligned} \quad (21)$$

The spatially-dependent functions δh and δB_{ρ} will be expanded in a Fourier series in the helical angle α . Allowing for all possible m values in $\alpha \equiv \zeta - (m/n)\theta$, a sinusoidal $e^{-i\omega t}$ time dependence and an arbitrary phase factor $\varphi_{m/n}$, the relevant Fourier series representation is

$$\delta h(\mathbf{x}, t) = \sum_{mn} \hat{\delta h}_{m/n}(\rho, \theta) e^{-i(n\alpha + \omega t - \varphi_{m/n})}, \quad (22)$$

$$\hat{\delta h}_{m/n} \equiv \int_{-\pi}^{\pi} \frac{d\alpha}{2\pi} e^{i(n\alpha + \omega t - \varphi_{m/n})} \delta h, \quad (23)$$

plus a similar Fourier representation for δB_{ρ} . Here, $\hat{\delta h}_{m/n}$ and $\delta \hat{B}_{\rho m/n}$ are real. Hence, the physical magnetic field perturbation can be written as

$$\delta B_{\rho}(\mathbf{x}, t) = \sum_{mn} \delta \hat{B}_{\rho m/n}(\rho, \theta) \cos(m\theta - n\zeta - \omega t + \varphi_{m/n}), \quad (24)$$

which is periodic in both the poloidal and toroidal angles.

Substituting Fourier series representations for δh and δB_{ρ} from (22) into (21), operating on the resultant equation with $(1/2\pi) \int_{-\pi}^{\pi} d\alpha e^{i(n'\alpha + \omega t - \varphi_{m/n'})}$ and defining $\omega_d \equiv (1/2\pi) \int_{-\pi}^{\pi} d\alpha e^{-i(n\alpha + \omega t - \varphi_{m/n})} \mathbf{v}_d \cdot \nabla \delta h / i \hat{\delta h}_{m/n}$ yields

$$\begin{aligned} \frac{v_{\parallel}}{B_0} (\mathbf{B}_0 \cdot \nabla \theta) \left[\frac{\partial \hat{\delta h}_{m/n}}{\partial \theta} + i(m - nq) \hat{\delta h}_{m/n} \right] \\ - i(\omega - \omega_d) \hat{\delta h}_{m/n} - \mathcal{C}\{\hat{\delta h}_{m/n}\} \\ = - \frac{v_{\parallel}}{B_0} \delta \hat{B}_{\rho m/n} f'_{Me}. \end{aligned} \quad (25)$$

The terms on the left side of (25) represent various physical effects: parallel bounce motion along the \mathbf{B}_0 field, parallel streaming in the sheared magnetic field when $m - nq \neq 0$, the Doppler frequency induced by the poloidal and toroidal flow of the plasma relative to the laboratory rest frame plus any externally imposed RMP frequency, the combination of the $\mathbf{B} \times \nabla \Phi_0$, gradient- B and curvature drift frequencies and finally the electron collisional damping rate. Their characteristic frequencies for untrapped (subscript u) thermal electrons are:

$\omega_u \simeq v_{Te}/R_0 q$, $(m - nq)\omega_u$, ω , $\omega_d \sim k_{\theta}(2T_e/eB_0R_0)$ and $\nu_{\text{eff}} \sim -\mathcal{C}\{\hat{\delta h}_{m/n}\}/\hat{\delta h}_{m/n}$.

In edge plasmas the electron collisional damping rate is usually much larger than the Doppler and drift frequencies. Thus, the bounce-average physics is dominated by the interplay between the collisional damping at rate ν_{eff} and the magnetic-shear-induced parallel streaming frequency $(m - nq)\omega_u \equiv k_{\parallel}(x)v_{Te}$; hence, there are no Landau-type resonances or effects. For the parameters in Appendix B, the approximate rates (s^{-1}) are: $\omega_u \simeq 3 \times 10^6$, $(m - nq)\omega_u \sim (0-8) \times 10^6$, $\omega \sim 10^4$, $\omega_d \sim 10^4$ and $\nu_{\text{eff}} \sim 2 \times 10^5$. Since the ω and ω_d frequencies are negligible relative to the other frequencies in (25), especially ν_{eff} , they will be neglected henceforth.

In (25) $v_{\parallel} \equiv \pm v \sqrt{1 - \lambda B_0(\rho, \theta)/B_{\text{max}}}$ is the parallel electron speed in which $v \equiv \sqrt{(2/m_e)(\varepsilon + e\Phi_0)}$ is the total speed, $\varepsilon \equiv m_e v_{\parallel}^2/2 + \mu B_0 - e\Phi_0$ is the total guiding center energy, $\mu \equiv m_e v_{\perp}^2/2B$ is the magnetic moment and $\lambda \equiv \mu B_{\text{max}}/\varepsilon$ is a dimensionless velocity-space pitch-angle variable. For untrapped electrons $0 \leq \lambda < 1$, while for trapped electrons $1 < \lambda \leq B_{\text{max}}/B_{\text{min}}$.

The first term in (25) will be annihilated by integrating over a bounce period using the operator $\oint dl/v_{\parallel} = \oint B_0 d\theta/(v_{\parallel} \mathbf{B}_0 \cdot \nabla \theta)$. Integrating over the cyclic trapped electron trajectories yields an equation for the trapped-particle δh_t in which the inhomogeneous term on the right vanishes; its solution requires δh_t to vanish. Physically, trapped particles don't carry any parallel flows over distances longer than the poloidal periodicity length.

Next, (25) will be integrated over the poloidal periodicity of untrapped electrons using a bounce-averaging operator $\int_{-\pi}^{\pi} d\theta B_0/(v_{\parallel} \mathbf{B}_0 \cdot \nabla \theta)$. Then, neglecting ω and ω_d , using a Lorentz scattering model electron Coulomb collision scattering operator $\mathcal{C}_L\{f(\varepsilon, \mu)\} = m_e v_{\parallel} \nu(v) (\partial/\partial\mu)[(\mu v_{\parallel}/B_0)(\partial f/\partial\mu)]$ in which $\nu(v) \equiv (4\pi n_e Z_{\text{eff}} e^4 \ln \Lambda)/(\{4\pi\epsilon_0\}^2 m_e^2 v^3)$ with $Z_{\text{eff}} \equiv \sum_i n_i Z_i^2/n_e$ is the Lorentz model collision frequency and dividing by $(B_{t0}/v) \int_{-\pi}^{\pi} d\theta/\mathbf{B}_0 \cdot \nabla \theta$ yields

$$\begin{aligned} ik_{\parallel} v \overline{\delta h}_u - 2\nu(v) \frac{B_{\text{max}}}{B_{t0}} \frac{\partial}{\partial \lambda} \left(\lambda \frac{\langle v_{\parallel} \rangle}{v} \frac{\partial \overline{\delta h}_u}{\partial \lambda} \right) \\ = -v \frac{\langle \delta \hat{B}_{\rho m/n} \rangle}{B_{t0}} f'_{Me}. \end{aligned} \quad (26)$$

Here, $\langle \dots \rangle$ indicates the flux surface average in (14).

The magnetic-shear-induced parallel wavenumber $k_{\parallel} \equiv -n[q(\rho) - m/n]/\bar{R}q(\rho) = k'_{\parallel}(\rho)x$ in which $k'_{\parallel}(\rho) \equiv -mq'(\rho)/[q^2(\rho)\bar{R}] = -k_{\theta}/L_S$ with poloidal wavenumber $k_{\theta} \equiv m/\rho$, local magnetic shear length $L_S \equiv \bar{R}q(\rho)/s(\rho)$, local shear parameter $s(\rho) = \rho q'(\rho)/q(\rho)$ and $q'(\rho) \equiv dq(\rho)/d\rho$. The radial distance off the rational surface is defined most generally by

$$x \equiv \frac{q(\rho) - m/n}{q'(\rho)} \simeq \rho - \rho_{m/n}. \quad (27)$$

In these formulas the FSA average major radius is $\bar{R} \equiv (B_{t0}/2\pi q) \int_{-\pi}^{\pi} d\theta/\mathbf{B}_0 \cdot \nabla \theta = (B_{t0}/2\pi I) \int_{-\pi}^{\pi} d\theta R^2 \simeq$

R_0 in which R_0 is the major radius of the magnetic axis. In (26) the poloidal-angle-averaged untrapped non-adiabatic distribution is $\overline{\delta h_u}(\rho, v, \lambda) \equiv (1/2\pi) \int_{-\pi}^{\pi} d\theta \delta \hat{h}_{m/n}$ and a $\langle \tilde{v}_{\parallel} \partial \overline{\delta h_u} / \partial \lambda \rangle \sim \mathcal{O}\{\epsilon^2\}$ term due to $\mathcal{O}\{\epsilon\}$ poloidal variations of v_{\parallel} and $\delta \hat{h}_{m/n}$ inside the collision operator has been neglected. The magnitude of the radial component of the m/n magnetic perturbation source term on the second line of (26) is

$$\langle \delta \hat{B}_{\rho m/n} \rangle \equiv \frac{\int_{-\pi}^{\pi} d\zeta \int_{-\pi}^{\pi} d\theta \frac{\delta \mathbf{B} \cdot \nabla \rho}{\mathbf{B}_0 \cdot \nabla \theta} e^{i(m\theta - n\zeta + \varphi_{m/n})}}{\int_{-\pi}^{\pi} d\zeta \int_{-\pi}^{\pi} \frac{d\theta}{\mathbf{B}_0 \cdot \nabla \theta}}, \quad (28)$$

which yields the usual definition for the ‘‘normal’’ (radial) projection of the m/n component of RMPs.^{13–15}

Since $\overline{\delta h_u}$ is a mostly separable function of its three independent variables, it is convenient to write it as

$$\overline{\delta h_u}(\rho, v, \lambda) \equiv -D(\rho) V(v, \rho) \Lambda(\lambda, x, v), \quad (29)$$

$$D(\rho) \equiv \langle \delta \hat{B}_{\rho m/n} \rangle / B_{t0}, \quad (30)$$

$$V(v, \rho) = [v/2\nu(v)] f'_{Me}. \quad (31)$$

Using this representation of $\overline{\delta h_u}$, the perturbed DKE (26) can be written as a second order partial differential equation for the pitch-angle function $\Lambda(\lambda)$:

$$\frac{\partial}{\partial \lambda} \left(\lambda \frac{\langle v_{\parallel} \rangle}{v} \frac{\partial \Lambda}{\partial \lambda} \right) - i \left(\frac{k_{\parallel}(x) v}{2\nu(v)} \frac{B_{t0}}{B_{\max}} \right) \Lambda = -1, \quad (32)$$

in which x and v are parameters. The boundary conditions (B.C.) for $\Lambda(\lambda)$ solutions of this differential equation are: 1) $\partial \Lambda / \partial \lambda$ finite at $\lambda = 0$ and 2) $\Lambda(\lambda = 1) = 0$, to connect smoothly to the trapped particle solution where the corresponding $\Lambda_t(\lambda) = 0$ for $1 < \lambda < B_{\max}/B_{\min}$.

B. RMP-induced parallel flows, radial fluxes

In terms of the v, λ velocity-space coordinates, the integral over the untrapped region of velocity space is $\int_u d^3v (\dots) = \sum_{\sigma} (\pi B_0 / B_{\max}) \int_0^{\infty} v^3 dv \int_0^1 d\lambda / |v_{\parallel}| (\dots)$ in which $\sigma \equiv \text{sign}\{v_{\parallel}\}$. Thus, the untrapped electron density perturbation induced by $\langle \delta \hat{B}_{\rho m/n} \rangle$ will be $\delta n_u \equiv \sum_{\sigma} (\pi B_0 / B_{\max}) \int_0^{\infty} v^3 dv \int_0^1 d\lambda \mathcal{R}e\{\delta f_e\} / |v_{\parallel}|$. As is evident from the v_{\parallel} symmetry properties of (26) and (32) and will be demonstrated explicitly below, the real part of $\overline{\delta h_u}$ is odd in v_{\parallel} . Hence, it does not contribute to δn_e and the perturbed electron density is just the adiabatic response $\delta n_e = n_{e0} e \delta \Phi / T_e$. A similar analysis for ions also yields an adiabatic response. The quasineutrality condition $0 = \sum_s q_s \delta n_s = (\sum_s n_s q_s^2 / T_s) \delta \Phi$ thus yields the requirement that $\delta \Phi = 0$. Hence, $\langle \delta \hat{B}_{\rho m/n} \rangle$ perturbations do not induce an electrostatic potential perturbation $\delta \Phi$ and the perturbed electron distribution is only due to the non-adiabatic contribution: $\delta f_e = \delta h$.

Since $\overline{\delta h_u}$ is odd in v_{\parallel} , the $\langle \delta \hat{B}_{\rho m/n} \rangle$ helical perturbations induce an electron flow and conductive heat flux parallel to the m/n helical pitch of the field lines:

$$\begin{aligned} \begin{bmatrix} n_e \delta V_{e\parallel t} \\ \delta q_{e\parallel t} / T_e \end{bmatrix} &= \int_u d^3v v_{\parallel} \begin{bmatrix} L_0^{(3/2)} \\ -L_1^{(3/2)} \end{bmatrix} \delta f_e \\ &= -\frac{B_0}{B_{\max}} 2\pi \int_0^{\infty} v^3 dv \left[\left(y - \frac{5}{2} \right) \right] \int_0^1 d\lambda |\mathcal{R}e\{\delta h_u\}|, \end{aligned} \quad (33)$$

in which $L_0^{(3/2)} \equiv 1$ and $L_1^{(3/2)} \equiv 5/2 - y$ are Laguerre polynomial functions of the normalized electron kinetic energy $y \equiv m_e v^2 / 2T_e$. Averaging the flows over poloidal angle θ [at constant helical angle $\alpha \equiv \zeta - (m/n)\theta$], again neglecting $\mathcal{O}\{\epsilon^2\}$ effects due to $\mathcal{O}\{\epsilon\}$ poloidal variations of B_0 and δh_u , and using for the Lorentz collision frequency $\nu(v) = (3\sqrt{\pi}/4) \nu_e (v_{Te}/v)^3$ and the representation of $\overline{\delta h_u}$ in (29), the poloidal-average of m/n helical flows in (33) induced by $\delta \hat{B}_{\rho m/n}^{\text{pl}}$ in the plasma are

$$\begin{aligned} \begin{bmatrix} n_e \overline{\delta V_{e\parallel t}} \\ \overline{\delta q_{e\parallel t}} / T_e \end{bmatrix} &= -n_e \frac{v_{Te}^2}{\nu_e} \frac{\langle \delta \hat{B}_{\rho m/n}^{\text{pl}} \rangle}{B_{t0}} \cos(n\alpha + \omega t - \varphi_{m/n}) \\ &\quad \times \begin{bmatrix} K_{00} & K_{01} \\ K_{10} & K_{11} \end{bmatrix} \cdot \begin{bmatrix} d \ln \hat{p}_e / d\rho \\ d \ln T_e / d\rho \end{bmatrix}, \end{aligned} \quad (34)$$

in which the dimensionless kinetic coefficients $K_{ij}(x)$ are

$$\begin{aligned} \begin{bmatrix} K_{00} & K_{01} \\ K_{10} & K_{11} \end{bmatrix} &= \frac{B_{t0}}{B_{\max}} \frac{2}{3\pi} \int_0^{\infty} dy y^3 e^{-y} \int_0^1 d\lambda |\mathcal{R}e\{\Lambda\}| \\ &\quad \times \begin{bmatrix} 1 & y - \frac{5}{2} \\ y - \frac{5}{2} & (y - \frac{5}{2})^2 \end{bmatrix}. \end{aligned} \quad (35)$$

The flux-surface-averaged radial electron density and conductive thermal fluxes induced by a single m/n component of the RMP-induced $\delta \mathbf{B}$ in the plasma can be calculated from the kinetic-based radial flux definitions:

$$\begin{aligned} \begin{bmatrix} \delta \Gamma_{et}^{m/n} \\ \delta \Upsilon_{et}^{m/n} / T_e \end{bmatrix} &\equiv \begin{bmatrix} \langle \delta \Gamma_{et} \cdot \nabla \rho \rangle \\ \langle \delta \mathbf{q}_{et} \cdot \nabla \rho \rangle / T_e \end{bmatrix} \\ &= \left\langle \int_u d^3v \delta f_e \begin{bmatrix} \left(y - \frac{5}{2} \right) \mathbf{v}_{\text{gc}} \cdot \nabla \rho \\ \left(y - \frac{5}{2} \right) v_{\parallel} \frac{\delta \mathbf{B}^{\text{pl}} \cdot \nabla \rho}{B_0} \end{bmatrix} \right\rangle \\ &= \left\langle \int_u d^3v \delta h_e \begin{bmatrix} \left(y - \frac{5}{2} \right) \mathbf{v}_{\parallel} \frac{\delta \mathbf{B}^{\text{pl}} \cdot \nabla \rho}{B_0} \end{bmatrix} \right\rangle \\ &= \left\langle \begin{bmatrix} n_e \overline{\delta V_{e\parallel t}} \\ \overline{\delta q_{e\parallel t}} / T_e \end{bmatrix} \frac{\delta \mathbf{B}^{\text{pl}} \cdot \nabla \rho}{B_{t0}} \right\rangle \\ &= -n_e \begin{bmatrix} D_{et}^{m/n} & D_T^{m/n} \\ \chi_n^{m/n} & \chi_{et}^{m/n} \end{bmatrix} \cdot \begin{bmatrix} d \ln \hat{p}_e / d\rho \\ d \ln T_e / d\rho \end{bmatrix}. \end{aligned} \quad (36)$$

Here, the matrix of radial transport diffusivities are

$$\begin{bmatrix} D_{et}^{m/n} & D_T^{m/n} \\ \chi_n^{m/n} & \chi_{et}^{m/n} \end{bmatrix} = \frac{v_{Te}^2}{\nu_e} \frac{1}{2} \left(\frac{\langle \delta \hat{B}_{\rho m/n}^{\text{pl}} \rangle}{B_{t0}} \right)^2 \begin{bmatrix} K_{00} & K_{01} \\ K_{10} & K_{11} \end{bmatrix}. \quad (37)$$

The radial electron density and heat fluxes in (36) are the same as the flutter-induced $\Gamma_{\mathbf{J} \times \mathbf{B}}$ in Eq. (112) of Ref. 25 and thermal flux Υ_{fl} in Eq. (58) of Ref. 26.

The effects of the various m/n helical $\delta \mathbf{B}$ components on the parallel flows and radial transport fluxes are independent. Thus, they have been calculated quasilinearly. Since the transport responses from various m/n RMPs usually overlap to some degree at each radius in the edge plasma, the total RMP-induced radial transport fluxes result from summing over all relevant m, n values:

$$\begin{bmatrix} \delta \Gamma_{\text{et}}^{\text{RMP}} \\ \delta \Upsilon_{\text{et}}^{\text{RMP}}/T_e \end{bmatrix} = -n_e \begin{bmatrix} D_{\text{et}}^{\text{RMP}} & D_T^{\text{RMP}} \\ \chi_n^{\text{RMP}} & \chi_{\text{et}}^{\text{RMP}} \end{bmatrix} \cdot \begin{bmatrix} d \ln \hat{p}_e/d\rho \\ d \ln T_e/d\rho \end{bmatrix}, \quad (38)$$

in which the total RMP-induced diffusivities are

$$\begin{bmatrix} D_{\text{et}}^{\text{RMP}} & D_T^{\text{RMP}} \\ \chi_n^{\text{RMP}} & \chi_{\text{et}}^{\text{RMP}} \end{bmatrix} = \sum_{mn} \begin{bmatrix} D_{\text{et}}^{m/n} & D_T^{m/n} \\ \chi_n^{m/n} & \chi_{\text{et}}^{m/n} \end{bmatrix}. \quad (39)$$

Because the K_{ij} matrix in (35) is symmetric, so are the RMP-induced diffusivity matrices in (37) and (39). Thus, the RMP-induced transport fluxes are Onsager-symmetric in terms of the thermodynamic forces $d \ln \hat{p}_e/d\rho \equiv d \ln p_e/d\rho - (e/T_e)(d\Phi_0/d\rho)$ and $d \ln T_e/d\rho$.

The toroidal model parallel fluxes and radial transport fluxes in (34)–(39) are analogous to the cylindrical model results¹⁹ that were summarized in (4)–(13). However, there are some key differences. The main one is that there are off-diagonal transport flux contributions due to the $D_T^{m/n}$ and $\chi_n^{m/n}$ coefficients in (36) and (38). Thus, the RMP-induced radial electron density flux includes an electron-temperature-gradient-driven flux contribution and the conductive electron thermal flux includes a pressure-gradient-driven contribution. In addition, definitions of various quantities are changed: the radial components of the RMP-induced magnetic perturbations ($\delta \hat{B}_{\rho m/n}^{\text{pl}} \rightarrow \langle \delta \hat{B}_{\rho m/n}^{\text{pl}} \rangle$), the spatial variation of the diffusivities [coefficient $G_c(x) \rightarrow K_{ij}(x)$ coefficients], the width of the region of maximum RMP-flutter-induced transport [$\delta_{\parallel c} \rightarrow \delta_{\parallel t}$ to be defined in (53) below], the reference parallel electron thermal diffusivity [$\chi_{\parallel c}^{\text{ref}} \rightarrow \chi_{\parallel t}^{\text{ref}}$ in (43) below] and the ratio of the density diffusivity to the electron thermal diffusivity ($2/5 \rightarrow K_{00}/K_{11}$).

Next, solutions of (32) for $\Lambda(\lambda, \rho, v)$ will be obtained and the K_{ij} coefficients determined in relevant asymptotic regimes, along with their regimes of validity. These results will then be stitched together to obtain the total magnetic-flutter-induced parallel electron flow $\delta \bar{V}_{e\parallel t}$ and conductive thermal flux $\delta \bar{q}_{e\parallel t}$, and resultant radial electron density and thermal fluxes $\delta \Gamma_{\text{et}}^{\text{RMP}}$ and $\delta \Upsilon_{\text{et}}^{\text{RMP}}$.

C. Solution for Λ near a rational surface ($k_{\parallel} \simeq 0$)

On and near the $q = m/n$ rational surface $k_{\parallel} \simeq 0$. Setting $k_{\parallel} = 0$ in (32) and integrating the resultant equation over λ from 0 to λ and then once again from λ to 1 using

the boundary condition $\delta h_u(\lambda=1) = 0$ to connect to the vanishing trapped particle solution yields

$$\Lambda_{k_{\parallel} \simeq 0}(\lambda) \equiv \int_{\lambda}^1 \frac{d\lambda'}{\langle v_{\parallel}(\lambda', \theta) \rangle / v}. \quad (40)$$

As noted earlier, this function is odd in the sign of v_{\parallel} . The pitch-angle integral in (35) of the $\Lambda_{k_{\parallel} \simeq 0}$ in (40) can be integrated by parts over λ to yield

$$\int_0^1 d\lambda \Lambda_{k_{\parallel} \simeq 0} = \int_0^1 \frac{\lambda d\lambda}{\langle \sqrt{1 - \lambda B/B_{\text{max}}} \rangle} \equiv \frac{4}{3} \frac{B_{\text{max}}^2}{\langle B_0^2 \rangle} f_c. \quad (41)$$

Here, f_c is the flow-weighted fraction of circulating (untrapped) particles that is well-known from neoclassical transport theory.²⁷ Since this result does not depend on v , performing the y (energy) integrals in (35) is straightforward. Neglecting $\mathcal{O}\{\epsilon^2\}$ effects so $\langle B_0^2 \rangle \simeq B_{t0}^2$ yields

$$\begin{bmatrix} K_{00} & K_{01} \\ K_{10} & K_{11} \end{bmatrix}_{k_{\parallel} \simeq 0} = \left(f_c \frac{B_{\text{max}}}{B_{t0}} \right) \frac{8}{9\pi} \begin{bmatrix} 6 & 9 \\ 9 & 75/2 \end{bmatrix}. \quad (42)$$

Thus, using $\chi_{\text{et}}^{m/n}$ from (37), the reference parallel diffusivity in (7) is changed for the toroidal model to

$$\chi_{\parallel t}^{\text{ref}} = K_{11 k_{\parallel} \simeq 0} \frac{v_{Te}^2}{\nu_e} = \left(f_c \frac{B_{\text{max}}}{B_{t0}} \right) \frac{100}{3\pi} \frac{v_{Te}^2}{\nu_e}. \quad (43)$$

The numerical coefficient in this toroidal model is an order of magnitude larger than the cylindrical model coefficient of $(5/4)(\langle n_u \rangle/n_0)^3$ in (7) — mainly because in the kinetic toroidal model a Lorentz model collision frequency with $\nu(v) \propto v^{-3}$ has been used which emphasizes contributions of suprathermal electrons in the Maxwellian distribution to parallel flows. In the toroidal model ($f_c B_{\text{max}}/B_{t0}$) replaces $(\langle n_u \rangle/n_0)^3$ as the factor that accounts for the fact that only untrapped electrons contribute to parallel flows. Setting the untrapped particle factor in (43) to unity yields the Lorentz model parallel electron thermal diffusivity of $\chi_{e\parallel}^L = (200/3\pi)(T_e/m_e \nu_e)$ which is 1.7 times the value Braginskii¹⁸ quotes for the $Z_i \rightarrow \infty$ Lorentz collision model limit. The ratio of the off-diagonal coefficients to $K_{00 k_{\parallel} \simeq 0}$ of 3/2 in (42) reflects the electron thermal force effect and its Onsager-symmetric frictional heat flux contribution, which in the Lorentz collision model limit is 3/2 instead of the usual 0.71 factor¹⁸ for $Z_i = 1$.

Using the results from (42) in the first row of (34) yields a parallel electron current density $\delta \bar{J}_{\parallel} = -n_e e \delta \bar{V}_{e\parallel t}$ for $k_{\parallel} \simeq 0$ induced by the m/n RMP-induced field of

$$\begin{aligned} \delta \bar{J}_{\parallel} &= \frac{1}{\eta_t^L} \langle \delta \hat{B}_{\rho m/n}^{\text{pl}} \rangle \cos(n\alpha + \omega t - \varphi_{m/n}) \\ &\times \frac{T_e}{e} \left[\left(\frac{d \ln p_e}{d\rho} - \frac{e}{T_e} \frac{d\Phi_0}{d\rho} \right) + \frac{3}{2} \frac{d \ln T_e}{d\rho} \right], \quad (44) \end{aligned}$$

in which the toroidal Lorentz model parallel resistivity is

$$\eta_t^L = \frac{1}{f_c B_{\text{max}}/B_{t0}} \frac{3\pi}{32} \frac{m_e \nu_e}{n_e e^2}. \quad (45)$$

When the untrapped particle factor $f_c B_{\max}/B_{t0}$ is set to unity, this is the usual Lorentz model collisional parallel electrical resistivity¹⁸ with numerical coefficient $3\pi/32 = 0.29$ for $Z_i \rightarrow \infty$. As can be seen from the form of (44), this $\overline{\delta J}_{\parallel}$ can be derived from the equilibrium parallel electron momentum equation. The T_e gradient contribution to (44) results from the electron parallel thermal force.

For the Appendix B parameters $\epsilon \simeq 0.33$ yields²⁸ $f_c \simeq 0.25$, and hence $(B_{\max}/B_{t0}) f_c \simeq 0.33$ which is about double the $(\langle n_u \rangle/n_0)^3$ value of about 0.17. The toroidal $\chi_{\parallel t}^{\text{ref}} \simeq 2.45 \times 10^{10} \text{ m}^2 \text{ s}^{-1}$ is about 17 times larger than the corresponding cylindrical result in (7). And the toroidal Lorentz model parallel resistivity is $\eta_t^L \simeq 0.9 m_e \nu_e / n_e e^2$.

D. Boundary layer solution off rational surface

To evaluate the RMP-induced effects off the m/n rational surface in the kinetic toroidal model, a solution of (32) is needed for $k_{\parallel} \neq 0$. For large k_{\parallel} the untrapped electron distribution solution of (32) for Λ will be localized in λ near the untrapped-trapped particle boundary where $\lambda \lesssim 1$. Thus, defining $\tilde{\lambda} \equiv 1 - \lambda$ and anticipating that $\tilde{\lambda} \ll 1$, the λ inside the collision operator in (32) can be approximated by unity and $\langle v_{\parallel}/v \rangle$ can be evaluated at $\lambda = 1$. Thus, in the large k_{\parallel} limit (32) becomes

$$\frac{\partial^2 \Lambda_{k_{\parallel} \neq 0}}{\partial \tilde{\lambda}^2} - i 2 k_{\lambda}^2 \frac{k_{\parallel}}{|k_{\parallel}|} \Lambda_{k_{\parallel} \neq 0} = - \frac{1}{\langle v_{\parallel}|_{\lambda=1}/v \rangle}, \quad (46)$$

in which the effective (large, complex) wavenumber is

$$k_{\lambda}(x, v) \equiv \left[\frac{|k_{\parallel}(x)| v (B_{t0}/B_{\max})}{4 \nu(v) |\langle v_{\parallel}|_{\lambda=1}/v \rangle} \right]^{1/2}. \quad (47)$$

Complementary solutions of the homogeneous part of (46) are of the form $e^{\pm \sqrt{\pm 2i} k_{\lambda} \tilde{\lambda}} = e^{\pm (1 \pm i) k_{\lambda} \tilde{\lambda}}$. The untrapped solution of (46) must vanish at the trapped particle boundary ($\lambda = 1$, $\tilde{\lambda} = 0$). For $k_{\lambda} \tilde{\lambda} \gg 1$ its real part must asymptotically vanish and have $\mathcal{I}m\{\Lambda_{k_{\parallel} \neq 0}\} = -(1/2 k_{\lambda}^2) (k_{\parallel}/|k_{\parallel}|) / \langle v_{\parallel}|_{\lambda=1}/v \rangle$. The boundary-layer-type particular solution of (46) that satisfies these B.C. is

$$\Lambda_{k_{\parallel} \neq 0} = - \frac{(i/2 k_{\lambda}^2) (k_{\parallel}/|k_{\parallel}|)}{\langle v_{\parallel}|_{\lambda=1}/v \rangle} \times \left[1 - e^{-k_{\lambda} \tilde{\lambda}} (\cos k_{\lambda} \tilde{\lambda} - i \frac{k_{\parallel}}{|k_{\parallel}|} \sin k_{\lambda} \tilde{\lambda}) \right]. \quad (48)$$

Since, as for the $k_{\parallel} \simeq 0$ solution in (40), this solution is odd in v_{\parallel} , $\delta n_e = n_{e0} e \delta \Phi / T_e$, which by quasineutrality requires $\delta \Phi = 0$. The pitch-angle integral in (34) of the $\Lambda_{k_{\parallel} \neq 0}$ in (48) can be integrated (for $k_{\lambda} \tilde{\lambda} \gg 1$) as follows:

$$\int_0^1 d\lambda \mathcal{R}e\{\Lambda_{k_{\parallel} \neq 0}\} = \frac{1}{2 k_{\lambda}^2 |\langle v_{\parallel}|_{\lambda=1}/v \rangle} \int_0^1 d\lambda e^{-k_{\lambda} \tilde{\lambda}} \sin k_{\lambda} \tilde{\lambda} \simeq \frac{1}{4 k_{\lambda}^3 |\langle v_{\parallel}|_{\lambda=1}/v \rangle}. \quad (49)$$

The criterion for the validity of the large k_{\parallel} solution in (48) is $k_{\lambda}(x, v) \gg 1$. Using the Lorentz model collision frequency $\nu(v) \equiv (3\sqrt{\pi}/4) \nu_e v_{Te}^3/v^3$, the effective wavenumber k_{λ} can be written as

$$k_{\lambda}(x, v) = |X|^{1/2} v^2/v_{Te}^2 = |X|^{1/2} y, \quad (50)$$

in which the normalized distance from $\rho_{m/n}$ is

$$X \equiv \frac{x}{\delta_{\parallel t}} = \frac{q(\rho) - m/n}{q'(\rho) \delta_{\parallel t}} \simeq \frac{\rho - \rho_{m/n}}{q'(\rho) \delta_{\parallel t}}. \quad (51)$$

Here, the toroidal magnetic-shear-influence width is

$$\delta_{\parallel t} \equiv \frac{c_t}{|k'_{\parallel}| \lambda_e} = c_t \frac{L_S}{k_{\theta} \lambda_e}, \quad (52)$$

$$c_t \equiv 3\sqrt{\pi} |\langle v_{\parallel}|_{\lambda=1}/v \rangle \frac{B_{\max}}{B_{t0}}. \quad (53)$$

For a model field $B_0(\theta) = B_{\max} - (B_{\max} - B_{\min}) \sin^2 \theta/2$, one can show that $|\langle v_{\parallel}|_{\lambda=1}/v \rangle| = \langle \sqrt{1 - B_0(\theta)/B_{\max}} \rangle \simeq (2/\pi) \sqrt{1 - B_{\min}/B_{\max}}$. For the parameters in Appendix B where $B_{\min}/B_{\max} \simeq 1/2$, this yields $|\langle v_{\parallel}|_{\lambda=1}/v \rangle| \simeq 0.45$. Hence, together with $B_{\max}/B_{t0} \simeq 4/3$ this gives $c_t \simeq 3.2$, which is about 2/3 of the analogous factor of $\sqrt{2} (n_0/\langle n_u \rangle)^2 \simeq 4.7$ obtained in (9) for the cylindrical model. For the parameters in Appendix B the characteristic radial layer width $\delta_{\parallel t}$ is about 0.146 cm.

Using the integral of Λ from (49) and the definition of k_{λ} from (50) in (35), the integrand of the integral over y in the matrix of K_{ij} coefficients for $k_{\parallel} \neq 0$ is just e^{-y} . Thus, performing the integrations over y in (35) yields

$$\begin{bmatrix} K_{00} & K_{01} \\ K_{10} & K_{11} \end{bmatrix}_{k_{\parallel} \neq 0} = \frac{1}{|X|^{3/2}} \frac{B_{t0}/B_{\max}}{\langle v_{\parallel}|_{\lambda=1}/v \rangle} \frac{1}{6\pi} \times \begin{bmatrix} 1 & -3/2 \\ -3/2 & 13/4 \end{bmatrix}. \quad (54)$$

This toroidal result for $k_{\parallel} \neq 0$ decreases as $|x|^{-3/2}$ with distance from the rational surface — because of the collisional boundary layer effects. Thus it decays more slowly than the cylindrical model's x^{-2} decay in (8).

E. Comprehensive radial transport fluxes

The $k_{\parallel} \neq 0$ solution in (48) is only valid asymptotically for $k_{\lambda} \gg 1$. Hence, using the definition of k_{λ} in (50), the $k_{\parallel} \neq 0$ solution in (48) is applicable for

$$y > 1/|X|^{1/2}, \quad \text{for } k_{\parallel} \neq 0 \text{ solution in (48)}. \quad (55)$$

When $k_{\lambda} < 1$, the pitch-angle “boundary layer” covers the entire untrapped particle region of velocity space. Then, the $k_{\parallel} \simeq 0$ solution is applicable. The $k_{\lambda} < 1$ criterion yields

$$y < 1/|X|^{1/2}, \quad \text{for } k_{\parallel} \simeq 0 \text{ solution in (40)}. \quad (56)$$

One additional constraint on the solution in (48) is that untrapped electrons must remain in a low collisionality regime where the effective electron collision frequency $\nu_{\text{eff}}^{k_\lambda}$ in the boundary layer is less than the bounce-averaged transit frequency $\langle\omega_u\rangle$ for the relevant untrapped electrons. The effective collision frequency in the boundary layer can be estimated from the bounce-averaged collision operator in (26): $\nu_{\text{eff}}^{k_\lambda} \simeq 2\nu(v) k_\lambda^2 (B_{\text{max}}/B_{t0}) \langle v_{\parallel} |_{\lambda=1} \rangle / v$. Since at the edge of this boundary layer $\lambda = 1$, the bounce-averaged transit frequency will be estimated to be $\langle\omega_u\rangle \simeq \langle v_{\parallel} |_{\lambda=1} \rangle / Rq$. Using these estimates, the criterion $\nu_{\text{eff}}^{k_\lambda} < \langle\omega_u\rangle$ can be reduced to

$$|X| < X_{\text{crit}} \equiv \frac{2}{3\sqrt{\pi}} \frac{B_{t0}}{B_{\text{max}}} \frac{\lambda_e(\rho)}{Rq(\rho)}. \quad (57)$$

For the pedestal parameters in Appendix B $X_{\text{crit}} \simeq 17$. The boundary layer constraint in (55) and the low collisionality constraint in (57) for the validity of the $k_{\parallel} \neq 0$ solution in (48) can be combined into a single constraint on the dimensionless electron energy variable:

$$y > y_{\text{min}} \equiv \max\{1/|X|^{1/2}, 1/X_{\text{crit}}^{1/2}\}. \quad (58)$$

The Λ solutions obtained in the preceding two subsections can be combined into a Padé approximate²⁹ form by energy smoothing³⁰ via integrating the solutions over their applicable energy ranges and adding the results. Doing so using the constraint conditions in (56) for the $k_{\parallel} \simeq 0$ solution in (40) and in (58) for the $k_{\parallel} \neq 0$ solution in (48) yields for the total toroidal model dimensionless kinetic coefficients [normalized via $(13/4) K_{11} k_{\parallel} \neq 0$]

$$\begin{bmatrix} K_{00} & K_{01} \\ K_{10} & K_{11} \end{bmatrix}_{\text{tot}} = \frac{B_{t0}/B_{\text{max}}}{\langle v_{\parallel} |_{\lambda=1} / v} \frac{13}{24\pi} \begin{bmatrix} G_{00} & G_{01} \\ G_{10} & G_{11} \end{bmatrix}, \quad (59)$$

in which the matrix $G_{ij}(x)$ of dimensionless, spatially dependent geometric coefficients is

$$\begin{bmatrix} G_{00} & G_{01} \\ G_{10} & G_{11} \end{bmatrix} = \frac{4}{13|X|^{3/2}} \times \left(\frac{|X|^{3/2}}{c_{\parallel t}} \int_0^{1/|X|^{1/2}} dy y^3 e^{-y} + \int_{y_{\text{min}}}^{\infty} dy e^{-y} \right) \begin{bmatrix} 1 & y - \frac{5}{2} \\ y - \frac{5}{2} & (y - \frac{5}{2})^2 \end{bmatrix}. \quad (60)$$

The $|X|^{3/2}/c_{\parallel t}$ coefficient of the first integral represents the ratio of the coefficient preceding the matrix in (42) to the corresponding one in (54), which yields

$$c_{\parallel t} = \frac{3}{16} \frac{B_{t0}^2/B_{\text{max}}^2}{f_c \langle v_{\parallel} |_{\lambda=1} / v}. \quad (61)$$

For Appendix B parameters this coefficient is about 0.94 and the coefficient of the G matrix in (59) is about 0.29.

The energy (y) integrals in (60) can be written in closed form but are rather complicated; hence they will not be written out here. The G_{ij} matrix coefficients are even functions of X . For $|X| \gg 1$ they decrease as $|x|^{-3/2}$, which indicates a slower decrease with increasing x than

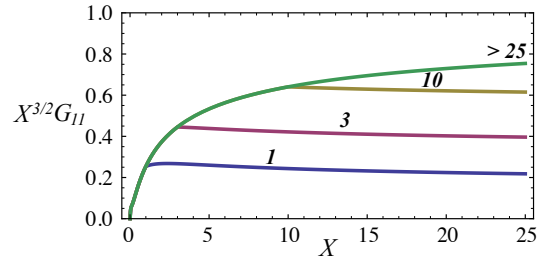


FIG. 1. Function $X^{3/2}G_{11}(X)$ for X_{crit} values of 1 (blue), 3 (red), 10 (yellow) and ≥ 25 (green) for $c_{\parallel t} = 0.94$.

the x^{-2} decrease in the cylindrical model indicated in (8). As Figure 1 shows, the G_{ij} matrix has been constructed so the radial electron heat flux coefficient $|X|^{3/2}G_{11}$ becomes unity in the $|X| \rightarrow \infty$ limit when $X_{\text{crit}} \rightarrow \infty$ ($y_{\text{min}} \rightarrow 1/|X|^{1/2}$). For small $|X|$, G_{11} is larger than unity. At the rational surface it becomes rather large: $\lim_{X \rightarrow 0} G_{11}(X) = 150/(13 c_{\parallel t})$ to yield the $\chi_{\parallel t}^{\text{ref}}$ in (43).

All the other $|X|^{3/2}G_{ij}$ coefficients are less than unity in the $|X| \rightarrow \infty$ limit. In particular, in this limit the ratio $G_{00}/G_{11} = 4/13$ for $X_{\text{crit}} \rightarrow \infty$. Thus, the ratio of the electron thermal to density diffusivity $\chi_{\text{et}}^{m/n}/D_{\text{et}}^{m/n}$ is about 3.25 in this limit, which is approximately applicable midway between rational surfaces. Also, whereas the ratio $D_T^{m/n}/D_{\text{et}}^{m/n}$ is 3/2 on a rational surface [see (42)], this ratio is about $-3/2$ midway between rational surfaces [see (54)]. Thus, the sign of the $d \ln T_e / d\rho$ contribution to the RMP-induced radial particle flux $\delta \Upsilon_{\text{et}}^{\text{RMP}}$ reverses sign and thus reduces it as one moves away from rational surfaces. Similarly, the pressure gradient thermodynamic force defined in (5) reduces the RMP-induced conductive radial electron heat flux $\delta \Upsilon_{\text{et}}^{\text{RMP}}$ midway between rational surfaces.

IV. DISCUSSION

The radial variations of the RMP-flutter-induced electron thermal diffusivities deduced from the toroidal and cylindrical models will now be compared for the DIII-D pedestal top parameters in Appendix B. The sum of the $\chi_e^{10/3}$ and $\chi_e^{11/3}$ diffusivities induced by 10/3 and 11/3 RMP fields will be illustrated in the $1/nq' \sim 2.8$ cm between these two rational surfaces in terms of the dimensionless radial variable $X \equiv x/\delta_{\parallel t}$ of the toroidal model. The cylindrical-based formula given in (12) will be used for the radial variation of the m/n RMP fields in the plasma for both the cylindrical and toroidal models. The resultant electron thermal diffusivities are shown in Fig. 2 for the cylindrical model with flow-screening factors f_{scr} of 4 (visco-resistive MHD model^{15,19}) and 30 (resistive MHD model^{13,14,19}), and for the toroidal model in the physically most relevant $f_{\text{scr}} = 4$ case.

The salient features of the radial profiles of the RMP-induced electron thermal diffusivities shown in Fig. 2 are

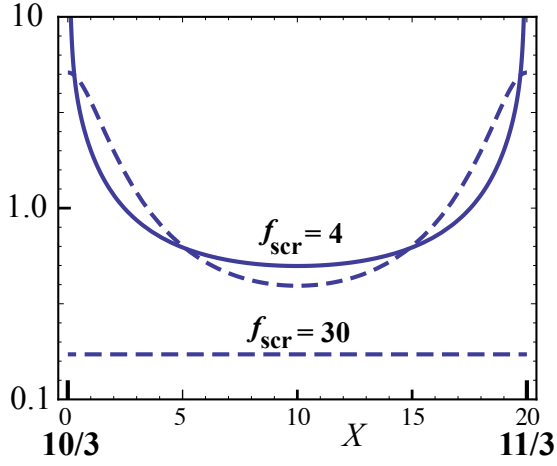


FIG. 2. Radial variation of $\chi_e^{10/3} + \chi_e^{11/3}$ for the cylindrical (dashed lines) and toroidal (solid line) model radial electron thermal diffusivities induced by the 10/3 and 11/3 RMP fields in the $\sim 1/nq' \simeq 2.8$ cm between their rational surfaces for the parameters in Appendix B. Here, $X \equiv x/\delta_{||t}$ is the normalized radial distance from the 10/3 rational surface.

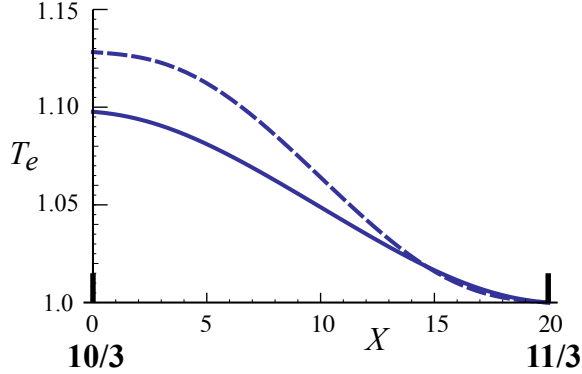


FIG. 3. Schematic illustration of the predicted electron temperature (keV) profiles in the $\sim 1/nq' \simeq 2.8$ cm between the 10/3 and 11/3 rational surfaces for the $f_{\text{scr}} = 4$ cylindrical (dashed line) and toroidal (solid line) model electron thermal diffusivities shown in Fig. 2.

as follows. In the cylindrical $f_{\text{scr}} = 30$ case χ_{ec}^{RMP} is spatially constant at a value of about 0.172 because the spatial variations of $G_c(x)$ and $\delta\hat{B}_{\rho m/n}^{\text{pl}}(x)$ cancel for the chosen parameters.¹⁹ On the rational surfaces ($|X| \rightarrow 0, 20$) the $f_{\text{scr}} = 4$ diffusivities are large — $\chi_{ec}^{m/n}(0) \simeq 5 \text{ m}^2 \text{ s}^{-1}$ for the cylindrical model and $\chi_{et}^{m/n}(0) \simeq 85 \text{ m}^2 \text{ s}^{-1}$ for the toroidal model. However, as shown in Fig. 3, while such large χ_e^{RMP} values flatten the T_e profile around rational surfaces, the average gradient of the T_e profile is determined mainly^{19,31} by the minimum thermal diffusivity between rational surfaces.

The minima midway between the 10/3 and 11/3 rational surfaces are only slightly different for the cylindrical and toroidal models: $\min\{\chi_{ec}^{\text{RMP}}\} \simeq 0.4 \text{ m}^2 \text{ s}^{-1}$

and $\min\{\chi_{et}^{\text{RMP}}\} \simeq 0.5 \text{ m}^2 \text{ s}^{-1}$. The spatially-averaged¹⁹ RMP-flutter-induced radial electron thermal diffusivities inferred from the $\Delta T_e/\Delta\rho$ changes they induce between the 10/3 and 11/3 surfaces are also only slightly different: $\bar{\chi}_{ec}^{\text{RMP}} \simeq 0.7 \text{ m}^2 \text{ s}^{-1}$ and $\bar{\chi}_{et}^{\text{RMP}} \simeq 0.9 \text{ m}^2 \text{ s}^{-1}$ for $f_{\text{scr}} \simeq 4$.

The RMP-flutter-induced $\bar{\chi}_e^{\text{RMP}} \sim 0.7\text{--}0.9 \text{ m}^2 \text{ s}^{-1}$ values estimated here for $f_{\text{scr}} = 4$ are slightly larger than the experimental $\chi_{e \text{ exp}}^{\text{sym}} \simeq 0.6 \text{ m}^2 \text{ s}^{-1}$ in the absence of RMPs at the top of DIII-D pedestals.¹⁹ If the effects of additional m/n RMP fields were added they would increase the estimated values slightly. However, the predicted $\bar{\chi}_e^{\text{RMP}}$ values would still be less than the RMP-induced experimentally inferred value¹⁹ of $\chi_{e \text{ exp}}^{\text{RMP}} \simeq 4 \text{ m}^2 \text{ s}^{-1}$. In addition, the experimentally observed^{11,12} $q_{95} \sim 3.5$ resonance sensitivity is not evident in the present estimates.

A key determining factor in these estimates is the use of the cylindrical-model-based flow-screened radial RMP-induced profile in (12). Recent M3D-C1¹⁵ fully toroidal two-fluid visco-resistive simulations by Ferraro³² indicate the flow-screened $\delta\hat{B}_{\rho m/n}^{\text{pl}}(x)$ profiles can increase to roughly their vacuum values before they reach the next rational surface. This implies that the k_θ factor in (12) should perhaps be replaced by $\gtrsim nq'$, which would increase the predicted $\bar{\chi}_e^{\text{RMP}}$ values by a factor of 2–4. Also, radial variations around the 10/3, 11/3 and 12/3 rational surfaces are apparently more complicated than (12) indicates. Thus, the most important factor for making detailed comparisons of this RMP-flutter-induced plasma transport model's predictions with experimental results is to use the numerical $\delta\hat{B}_{\rho m/n}^{\text{pl}}(x)$ profiles^{15,32} in evaluating the $\chi_e^{m/n}$ formulas in (11) and (37).

The preceding discussion assumed that RMP-flutter-induced radial plasma transport occurs throughout the region between the 10/3 and 11/3 rational surfaces and that if magnetic islands are present at either of these rational surfaces they have negligible widths. While magnetic islands of half width $W/2$ (~ 0.7 cm, $X_{W/2} \sim 5$ for $f_{\text{scr}} = 4$) bifurcate the magnetic topology²² and dramatically increase the effective radial plasma transport near rational surfaces,³³ the RMP-induced T_e gradient midway between rational surfaces is not affected much. Thus, the presence of non-overlapping magnetic islands at the rational surfaces would probably reduce the average $\Delta T_e/\Delta\rho$ somewhat. However, they would not change the overall conclusion here that the radially-averaged $\bar{\chi}_e^{\text{RMP}}$ is determined mainly by the minimum electron thermal diffusivity midway between rational surfaces.

The RMP-induced flutter can also have other effects on plasma transport in the edge of tokamak plasmas. Because parallel flows are proportional to the parallel diffusivities, the corresponding RMP-induced ion parallel flows and radial fluxes will be smaller than those for electrons by a factor of $(v_{Ti}^2/\nu_i)/(v_{Te}^2/\nu_e) \sim (m_e/m_i)^{1/2}(T_i/T_e)^{5/2} \sim 1/60$ and hence are negligible. Thus, the RMP-induced radially outward electron density flux $\delta\Gamma_e^{\text{RMP}}$ causes an inward radial current density $\delta J_\rho^{\text{RMP}} = -e\delta\Gamma_e^{\text{RMP}}$. This causes a co-current toroidal

torque density on the plasma of $\delta T_\zeta = e \delta \Gamma_e^{\text{RMP}} \psi'_p > 0$, which results from a $\langle \mathbf{e}_\zeta \cdot \overline{\delta \mathbf{J}_\parallel \times \delta \mathbf{B}_\perp} \rangle$ term in Ref. 25, in which $\mathbf{e}_\zeta \equiv R^2 \nabla \zeta = R \hat{\mathbf{e}}_\zeta$ is the covariant base vector. This process produces a quasilinear-type toroidal torque density on the edge plasma in the co-current direction, which would increase plasma toroidal rotation there. This is qualitatively consistent with the RMP-induced increases in the toroidal rotation of the carbon impurity component observed in DIII-D — see Fig. 6h in Ref. 11 and Fig. 4.19b in Ref. 20.

These RMP-induced torque effects are not included in the present linear calculations^{13–15} of the RMP-induced fields in the edge plasma. Thus, the present analysis is not self-consistent. Exploration of these nonlinear RMP-flutter-induced plasma transport and torque effects on the $\delta \hat{B}_{\rho m/n}^{\text{pl}}(x)$ profiles, magnetic reconnection and formation of magnetic islands is left for future work.

V. SUMMARY

This paper has developed a kinetic, toroidal model of plasma transport induced by externally applied resonant magnetic perturbations outside magnetic islands at rational surfaces. To lowest order the ideal MHD constraint requires $\mathbf{B} \cdot \nabla T_e \simeq 0$ which causes the fluid collisional¹⁸ parallel electron heat flux $\mathbf{q}_{e\parallel}$ to vanish. However, the kinetic effects of electron collisional damping in combination with RMP-induced spatial flutter produce a higher order $\delta q_{e\parallel} \neq 0$ and $\mathbf{B} \cdot \nabla T_e^{\nu_e} \neq 0$. The physics and irreversible processes responsible for transport are discussed in the Introduction and Appendix A.

The RMP-flutter-induced radial electron density and heat transport fluxes are given in (38), for which diffusivity coefficients are specified in (37), (39), (59) and (60). Also, as discussed in the preceding Section, since the corresponding ion fluxes are negligible, the outward non-ambipolar radial electron density flux creates a radial current density which usually induces a co-current toroidal torque density on the edge plasma.

These toroidal model results are qualitatively similar to the previously derived cylindrical model results.¹⁹ Most of the results are quantitatively less than a factor of two different for the DIII-D pedestal top parameters in Appendix B — except for $\chi_{\parallel t}^{\text{ref}}$ in (43) which is more than order of magnitude larger than $\chi_{\parallel c}^{\text{ref}}$ in (7), mainly because a Lorentz collision frequency $\nu(v) \sim 1/v^3$ is used in the toroidal model. Some of the main physics-based differences are: the $\nu(v) \sim 1/v^3$ used in the toroidal model causes the plasma transport fluxes in (38) to have “off-diagonal” contributions in contrast to the “diagonal” cylindrical model fluxes in (10); the f_c factor in (43) represents the fact that only circulating particles carry parallel flows in low collisionality plasmas; the toroidal model magnetic-shear-influence width $\delta_{\parallel t}$ defined in (53) scales differently with aspect ratio and is somewhat smaller than the $\delta_{\parallel c}$ in (9); and, far from rational surfaces the

toroidal model geometric factor $G_{ij} \sim 1/|x|^{3/2}$ in (60) decreases more slowly than the cylindrical model $G_c \sim 1/x^2$ in (8) — because of the kinetic-based boundary-layer effects in the pitch-angle distribution given in (48).

The radial variation of the RMP-flutter-induced radial electron thermal diffusivities in the toroidal and cylindrical models are illustrated in Fig. 2. While they differ significantly near rational surfaces and spatially, Fig. 3 shows their effects on the T_e profiles are similar. The radially-averaged¹⁹ RMP-induced radial electron thermal diffusivity is determined primarily by the minimum diffusivity midway between rational surfaces.

The RMP-flutter-induced electron thermal diffusivity at the top of DIII-D H-mode pedestals is estimated to be slightly larger than the corresponding diffusivity before RMPs are applied. See Section IV and Ref. 19 for more details on comparisons with DIII-D data. Thus, the RMP-flutter-induced electron transport should reduce the T_e and n_e gradients at the pedestal top. These decreases reduce the pressure-gradient-drive for peeling-ballooning instabilities and can thus contribute significantly to suppression of ELMs in these discharges.^{10,11}

More precise quantitative comparisons with experimental results will require numerical evaluations using detailed flow-screened RMP-induced radial magnetic perturbations $\delta \hat{B}_{\rho m/n}^{\text{pl}}(x)$ in the edge plasma obtained from linear two-fluid MHD modeling.¹⁵ Also, consideration of the quasilinear toroidal torque density induced by the RMPs and its effects on plasma toroidal rotation (and hence radial electric field²⁵) are left for future work.

ACKNOWLEDGMENTS

The authors are grateful to T.E. Evans and many other colleagues in the DIII-D program for useful discussions of RMP effects on H-mode pedestals. They are particularly grateful to S. Mordijck for providing details of her transport analyses²⁰ of relevant DIII-D pedestals,¹¹ to N.M. Ferraro for developing information on two-fluid computations^{15,32} of RMP-induced perturbations in these toroidally rotating DIII-D plasmas and to P.T. Raum and S.P. Smith for some model clarifications that resulted from their numerical evaluations of the model for comparisons with DIII-D data.

This research was supported by DoE grant DE-FG02-86ER53218 and motivated by work on DE-FG02-92ER54139.

Appendix A: Irreversibility in and validity conditions for the flutter transport model

Collision-induced irreversibility is critical for producing RMP-flutter-induced radial plasma transport. It is manifested through the finite electron-collision-induced parallel electron thermal and density diffusivities and fluxes. These effects on the T_e profile near a rational

surface will be illustrated by first considering the effects of an infinitely large (collisionless) parallel electron thermal diffusivity using a cylindrical model. Then, the kinetic-based effects of an electron collision damping rate ν_e that is comparable to the free-streaming frequency $k_{\parallel}(x)v_{Te}$ will be considered and related to the cylindrical model results developed previously¹⁹ (see Section II). In particular this appendix discusses, for field lines outside any island at the m/n rational surface, how electron collisions cause a finite $\delta\mathbf{q}_{e\parallel} \neq 0$ and consequently a small $\mathbf{B} \cdot \nabla T_e^{\nu_e} \neq 0$, and why the radial gradient of T_e and the lowest order electron Maxwellian distribution are just functions of ρ , i.e., $\nabla T_e \simeq \nabla \rho dT_e/d\rho$ and $\nabla f_{Me} \simeq \nabla \rho df_{Me}/d\rho$ so $\delta\mathbf{B} \cdot \nabla f_{Me} \simeq \delta B_{\rho} df_{Me}/d\rho$.

The collisional Braginskii¹⁸ parallel electron conductive heat flux is

$$\mathbf{q}_{e\parallel} \equiv -n_e \chi_{e\parallel} \frac{\mathbf{B}\mathbf{B}}{B^2} \cdot \nabla T_e = -n_e \chi_{e\parallel} \frac{\mathbf{B}}{B} \nabla_{\parallel} T_e. \quad (\text{A1})$$

Near the $q = m/n$ rational surface the $\delta\mathbf{B}_{r\,m/n}$ magnetic perturbation is usually dominant. Then, using the local helical variables r, θ, α in which $\alpha \equiv \zeta - (m/n)\theta$ and a total magnetic field $\mathbf{B} = \mathbf{B}_0 + \delta\mathbf{B}_{m/n}$, the parallel gradient of T_e can be written for the cylindrical model as [see discussion preceding Eq. (21)]

$$\begin{aligned} B\nabla_{\parallel} T_e &\equiv \mathbf{B} \cdot \nabla T_e = \mathbf{B}_0 \cdot \nabla T_e + \delta\mathbf{B}_{m/n} \cdot \nabla T_e \\ &= \mathbf{B}_0 \cdot \nabla \theta \left(q - \frac{m}{n} \right) \frac{\partial T_e}{\partial \alpha} + \delta\mathbf{B}_{m/n} \cdot \nabla T_e \\ &\simeq -\frac{k_{\parallel}(x)}{n} B_0 \frac{\partial T_e}{\partial \alpha} + \delta\mathbf{B}_{m/n} \cdot \nabla T_e. \end{aligned} \quad (\text{A2})$$

The last form is obtained using $\mathbf{B}_0 \cdot \nabla \theta / B_0 \simeq 1/R_0 q$ and $k_{\parallel}(x) \equiv -(q - m/n)/R_0 q \simeq -nq'/R_0 q = -k_{\theta} x / L_S$.

Neglecting local sources and sinks, the flux surface average (FSA) equilibrium electron energy balance equation in the vicinity of a rational surface becomes $\langle \nabla \cdot \mathbf{q}_e \rangle \simeq 0$. In the limit where collisional parallel electron heat transport is large compared to perpendicular electron heat transport, this becomes simply

$$\begin{aligned} 0 &\simeq \langle \nabla \cdot \mathbf{q}_{e\parallel} \rangle = \frac{1}{r} \frac{d}{dr} \left[r \langle \mathbf{q}_{e\parallel} \cdot \hat{\mathbf{e}}_r \rangle \right] \\ &= -\frac{1}{r} \frac{d}{dr} \left[r \left\langle \frac{\hat{\mathbf{e}}_r \cdot \delta\mathbf{B}}{B_0} n_e \chi_{e\parallel} \nabla_{\parallel} T_e \right\rangle \right], \end{aligned} \quad (\text{A3})$$

in which $\hat{\mathbf{e}}_r \equiv \nabla r$ is a unit vector in the radial direction.

In the collisionless limit where $\chi_{e\parallel} \rightarrow \infty$, (A3) is satisfied by setting the $\nabla_{\parallel} T_e$ in (A2) to zero. Assuming $T_e \equiv T_{e0}(r) + \delta T_e(r, \alpha)$ and a radial magnetic perturbation $\delta\mathbf{B}_{r\,m/n} \equiv \hat{\mathbf{e}}_r \cdot \delta\mathbf{B}_{m/n} = \delta\hat{B}_{r\,m/n} \cos(n\alpha)$, the $B\nabla_{\parallel} T_e = \mathbf{B}_0 \cdot \nabla \delta T_e + \delta\mathbf{B}_{m/n} \cdot \nabla T_e = 0$ condition is

$$-\frac{k_{\parallel}(x)}{n} \frac{\partial \delta T_e}{\partial \alpha} + \frac{\delta\hat{B}_{r\,m/n}}{B_0} \cos(n\alpha) \frac{\partial}{\partial r} [T_{e0} + \delta T_e] = 0. \quad (\text{A4})$$

Neglecting $\partial \delta T_e / \partial r$ and using the boundary condition that δT_e should vanish if $\delta\hat{B}_{r\,m/n}$ vanishes, this equation

can be integrated over α to yield

$$\delta T_e(r, \alpha) \simeq \frac{1}{k_{\parallel}(x)} \frac{\delta\hat{B}_{r\,m/n}}{B_0} \sin(n\alpha) \frac{dT_{e0}}{dr}, \quad (\text{A5})$$

which is likely to be too small and radially localized to be experimentally observable.

The nonlinear term $\delta\hat{B}_{r\,m/n} |d\delta T_e/dr|$ in (A4) is negligible in obtaining (A5) from (A4) if

$$|dT_{e0}/dr| \gg |d\delta T_e/dr|, \quad (\text{A6})$$

which yields the condition

$$|x| \gg x_c \equiv \left[\frac{\delta\hat{B}_{r\,m/n}(r_{m/n})}{B_0} \frac{L_S}{k_{\theta}} \right]^{1/2} = \frac{W}{4}. \quad (\text{A7})$$

Here, W is the width²² of the magnetic island produced by the $\delta\hat{B}_{r\,m/n}$ helical magnetic perturbation at the rational surface that results from magnetic reconnection there. Physically, this condition indicates the flutter transport analysis will only be valid outside any island around the m/n rational surface. This is also the validity condition for the radial field line flutter equation in (1). For the DIII-D pedestal top parameters given in Appendix B, $x_c \simeq 0.36$ cm for a flow-screening factor $f_{\text{scr}} = 4$ while for $f_{\text{scr}} = 30$ one obtains $x_c \simeq 0.13$ cm.

The $\delta T_e(r, \alpha)$ solution in (A5) represents the effect of advection of the electron temperature by the ideal MHD magnetic field perturbation $\delta\mathbf{B} = \nabla \times (\delta\xi \times \mathbf{B}_0)$ induced by a fluid perturbation $\delta\xi$. To see this note first that an incompressible fluid perturbation $\delta\xi = \hat{\mathbf{e}}_r \delta\xi_r \sin(-n\alpha)$ causes a $\delta B_{r\,m/n} \equiv \hat{\mathbf{e}}_r \cdot \delta\mathbf{B} \simeq (\mathbf{B}_0 \cdot \nabla)(\hat{\mathbf{e}}_r \cdot \delta\xi) \simeq k_{\parallel}(x) \cos(-n\alpha) B_0 \delta\hat{\xi}_r$. On a helically perturbed (but still closed) magnetic flux surface $T_e(\mathbf{x} + \delta\xi) \simeq T_{e0}(r) + \delta\xi_r dT_{e0}/dr = \text{constant}$. Note that since $-n\alpha = k_{\parallel}(x)\ell$, the fluid displacement $\delta\xi_r = (\delta\hat{B}_{r\,m/n}/B_0)[\sin(-n\alpha)/k_{\parallel}]$ is the same as the radial field line excursion $\delta x \equiv x - x_0$ in (1). The radial fluid perturbation $\delta\xi_r$ induces the T_e perturbation $\delta\xi_r dT_{e0}/dr \simeq -(1/k_{\parallel})(\delta\hat{B}_{r\,m/n}/B_0) \sin(n\alpha) dT_{e0}/dr$, which has the opposite sign of the $\delta T_e(r, \alpha)$ in (A5) which is the $\delta T_e \sim -(\mathbf{B}_0 \cdot \nabla)^{-1} \delta\mathbf{B} \cdot \nabla T_e$ required for obtaining $\mathbf{B} \cdot \nabla T_e = 0$.

In the collisionless limit it is $\chi_{e\parallel} \sim 1/\nu_e \rightarrow \infty$ which enforces $\mathbf{B} \cdot \nabla T_e \rightarrow 0$. Then, T_e is constant along the total magnetic field $\mathbf{B} = \mathbf{B}_0 + \delta\mathbf{B}$ and $\mathbf{q}_{e\parallel} = 0$. This is the ideal MHD limit in which the ‘‘frozen flux theorem’’ requires electrons and the entire electron fluid to move together with the magnetic field as it is perturbed. However, this is a singular limit since from (A1) $-\mathbf{q}_{e\parallel}/n_e = (\mathbf{B}/B) \chi_{e\parallel} \nabla_{\parallel} T_e \rightarrow \infty \times 0$, which is taken to be zero in ideal MHD. This singular limit is resolved by electron collisions, whose effects will be discussed next.

In contrast to ideal MHD, in dissipative fluid models electron collisions facilitate irreversible parallel flows and radial electron motion relative to the magnetic field. They do this via a combination of the electrical resistivity in the parallel electron momentum equation (Ohm’s

law) which causes slippage of the electron fluid through magnetic field lines and finite parallel electron heat flux in the electron energy balance equation. These electron collisional effects resolve the singular behavior and allow $\delta\mathbf{B}_{m/n}$ perturbations to produce a finite $\delta q_{e\parallel}$ near m/n rational surfaces when $\chi_{e\parallel}$ is finite, not infinite.

For example, the parallel component of the perturbed collisional heat flux equation is given by $0 = -v_{Te}^2 n_e \nabla_{\parallel} T_e - \nu_e \delta q_{e\parallel}$. While to lowest order in ν_e this relation requires $\nabla_{\parallel} T_e \rightarrow 0$, electron collisions cause the higher order $\nabla_{\parallel} T_e^{\nu_e}$ to be nonzero when $\delta q_{e\parallel} \neq 0$. Thus, outside any magnetic island at the m/n rational surface, to lowest order T_e is just advected by the ideal MHD fluid perturbation $\delta\xi_r = x - x_0$, but at higher order electron collisions cause $\delta q_{e\parallel} \neq 0$ and $\nabla_{\parallel} T_e^{\nu_e} \neq 0$. Since $\delta T_e \sim \sin n\alpha$ and $\delta q_{e\parallel} \sim \delta B_{\rho m/n} \sim \cos n\alpha$ are different out of phase fluid moments and both are unknowns, a kinetic-based description is needed to determine the effects of ν_e on the higher order relationship between $\delta q_{e\parallel}$ and $\nabla_{\parallel} T_e^{\nu_e}$.

Kinetic distortions of the electron distribution away from a lowest order Maxwellian distribution f_{Me} are caused by the parallel motion of the electron guiding centers along the radially fluttering RMP field $\delta\mathbf{B}$: $d\delta f_e/dt \sim -(v_{\parallel}/B_0)\delta\mathbf{B}\cdot\nabla f_{Me}$ — see Eqs. (15)–(18). The question then is: what does ∇f_{Me} depend on? This can be determined by exploring the r, α dependence of $\nabla T_e = \hat{\mathbf{e}}_r(\hat{\mathbf{e}}_r\cdot\nabla T_e) + \hat{\mathbf{e}}_{\alpha}(\hat{\mathbf{e}}_{\alpha}\cdot\nabla T_e)$. As indicated in (A6), when the condition in (A7) is satisfied the radial gradient of δT_e is negligible and hence $\hat{\mathbf{e}}_r\cdot\nabla T_e \simeq dT_{e0}/dr$. Further, $\hat{\mathbf{e}}_{\alpha}\cdot\nabla\delta T_e$ is negligible compared to the lowest order dT_{e0}/dr for $x > L_S(\delta\hat{B}_{r m/n}/B_0)$, which is generally a less stringent condition than (A7). Thus, under these conditions $\nabla T_e \simeq \hat{\mathbf{e}}_r dT_{e0}(r)/dr$. Hence, as long as the condition in (A7) is satisfied f_{Me} will only be a function of r or ρ and $\delta\mathbf{B}\cdot\nabla f_{Me} \simeq \delta B_{r m/n} df_{Me}/dr$, as derived in (16) from the lowest order drift kinetic equation.

The kinetic-based electron collisional damping effects can be illustrated by analyzing the solution of the bounce-averaged Eq. (26). Representing the Lorentz electron collision operator in this equation by $-\nu_{\text{eff}}\delta\bar{h}_u$ and re-inserting the frequency ω , Eq. (26) becomes

$$[\nu_{\text{eff}} + i(k_{\parallel}\sigma v - \omega)]\delta\bar{h}_u + (\sigma v/B_0)\langle\delta\mathbf{B}_{m/n}\cdot\nabla f_{Me}\rangle = 0, \quad (\text{A8})$$

in which $\sigma = \text{sign}\{v_{\parallel}\}$. The physically relevant solution of this equation is of the form

$$\mathcal{R}e\{\delta\bar{h}_u\} = -\mathcal{R}e\left\{\frac{(\sigma v/B_0)\langle\delta\mathbf{B}_{m/n}\cdot\nabla f_{Me}\rangle}{\nu_{\text{eff}} + i[k_{\parallel}(x)\sigma v - \omega]}\right\}. \quad (\text{A9})$$

In the collisionless limit this solution is singular and an electron Landau-type resonance occurs. This produces a response that is finite within a distance $x_L \sim \omega L_S/(k_{\parallel}v_{Te})$ (~ 0.01 cm for Appendix B parameters) of a rational surface but is exponentially small outside this extremely narrow region. The collisionless ideal MHD analysis above effectively neglects this very thin layer and thus concludes that $q_{e\parallel} \rightarrow 0$ everywhere as $\nu_{\text{eff}} \rightarrow 0$.

However, at the top of H-mode pedestals with parameters like those in Appendix B the effective electron collision damping rate ν_{eff} is comparable to the RMP-induced magnetic shear streaming frequency $k_{\parallel}(x)v_{Te}$ and both are much larger than ω . Then, the energy flux moment of the solution in (A9) with $v \rightarrow v_{Te}$ yields $\delta q_{e\parallel}^{\text{eff}} = -n_e\chi_{e\parallel}^{\text{eff}}(x)(\delta B_{r m/n}(\mathbf{x}, t)/B_0)(dT_{e0}/dr)$ in which $\chi_{e\parallel}^{\text{eff}}(x) \sim v_{Te}^2\nu_{\text{eff}}/[k_{\parallel}^2(x)v_{Te}^2 + \nu_{\text{eff}}^2] \sim \chi_{ec}^{\text{ref}}/(1+x^2/\delta_{\parallel c}^2)$. Equating this to $q_{e\parallel} \equiv -n_e(v_{Te}^2/\nu_e)\nabla_{\parallel}T_e$ implies that $\nabla_{\parallel}T_e^{\nu_e} \sim (\delta B_{r m/n}/B_0)(\langle n_u \rangle/n_0)^3/(1+x^2/\delta_{\parallel c}^2)(dT_{e0}/dr)$, which is both smaller than $\nabla_{\parallel}\delta T_e$ and proportional to the electron collision frequency ν_e in the physically most important region where $|x| \gg \delta_{\parallel}$.

Thus, electron collisional damping resolves the ideal MHD singularity near rational surfaces induced by RMPs. It also produces a finite parallel conductive heat flux $\delta q_{e\parallel}$ along the total $\mathbf{B} = \mathbf{B}_0 + \delta\mathbf{B}$ helical field lines and a nonzero $\nabla_{\parallel}T_e^{\nu_e}$ which is smaller than the characteristic magnitude of the ideal MHD $\nabla_{\parallel}T_e \sim (1/B)(\mathbf{B}_0\cdot\nabla\delta T_e)$ defined in (A5). These electron collision effects on the RMP-flutter-induced parallel electron heat flux and radial electron heat transport are what have been calculated more precisely in Ref. 19 for a cylindrical model (see Section II) and in Section III for the kinetic toroidal model, assuming the condition in (A7) is satisfied.

Appendix B: H-mode pedestal, RMP parameters

The Braginskii¹⁸ collisional parallel electron thermal diffusivity for a purely hydrogenic ($Z_i = 1$) ion plasma is $\chi_{e\parallel} \simeq 3.2(T_e/m_e\nu_e) = 1.6v_{Te}^2/\nu_e$ in which $v_{Te} \equiv \sqrt{2T_e/m_e}$ is the electron thermal speed, $\nu_e \simeq 5 \times 10^{-11}(n_e Z_{\text{eff}}/[T_e(\text{eV})]^{3/2})(\ln\Lambda/17)$ s⁻¹ is the electron collision frequency and $\lambda_e \equiv v_{Te}/\nu_e \simeq 1.2 \times 10^{-20}[T_e(\text{eV})]^2/[n_e(\text{m}^{-3})Z_{\text{eff}}(\ln\Lambda/17)]$ m is the electron collision length in which Z_{eff} is the effective ion charge $Z_{\text{eff}} \equiv \sum_i n_i Z_i^2/n_e$. These plasma, and relevant magnetic and geometric parameters in the top [at $\Psi_N \equiv \psi_p(\rho)/\psi_p(a) = 0.95$] of a typical DIII-D H-mode pedestal in which RMP fields suppress ELMS^{11,19,20} are listed in Table I. The usual $Z_i = 1$ Braginskii¹⁸ collisional parallel electron heat diffusivity is $\chi_{e\parallel} \simeq 10^{10}$ m²s⁻¹ for the parameters in Table I.

REFERENCES

- ¹C.C. Hegna, J.W. Connor, R.J. Hastie and H.R. Wilson, Phys. Plasmas **3**, 584 (1996).
- ²J.W. Connor, R.J. Hastie, H.R. Wilson and R.L. Miller, Phys. Plasmas **5**, 2687 (1998).
- ³H.R. Wilson, P.B. Snyder, G.T.A. Huysmans and R.L. Miller, Phys. Plasmas **9**, 1277 (2002).
- ⁴P.B. Snyder, H.R. Wilson, J.R. Ferron, L.L. Lao, A.W. Leonard, T.H. Osborne, A.D. Turnbull, D. Mossessian,

TABLE I. Parameters at $\Psi_N = 0.95$ in the top of an H-mode pedestal in DIII-D when $n = 3$ RMPs suppress ELMs.^{11,19,20}

Parameter	symbol	value
electron temperature	T_e	1130 eV
electron density	n_e	$2.5 \times 10^{19} \text{ m}^{-3}$
effective ion charge	Z_{eff}	1.7
electron thermal speed	v_{Te}	$2 \times 10^7 \text{ m s}^{-1}$
electron collision frequency	ν_e	$5.7 \times 10^4 \text{ s}^{-1}$
electron collision length	$\lambda_e \equiv v_{Te}/\nu_e$	350 m
reference \parallel thermal diffusivity	v_{Te}^2/ν_e	$7 \times 10^9 \text{ m}^2 \text{ s}^{-1}$
average major radius	$\bar{R} \simeq R_0$	1.7 m
average separatrix radius	a	0.79 m
average local minor radius	ρ, ρ_N	0.735 m, 0.93
“safety factor”	$q_{95} \equiv q(\Psi_N)$	3.5
magnetic shear parameters	$q', s \equiv \rho q'/q$	$12 \text{ m}^{-1}, 2.5$
magnetic shear length	$L_S \equiv \bar{R}q/s$	2.4 m
effective poloidal wavenumber	$k_\theta \equiv m/\rho$	15 m^{-1}
magnetic field variation factor	$B_{\text{max}}/B_{\text{min}}$	2
inverse magnetic aspect ratio	$\epsilon \equiv \Delta B/2B_{t0}$	0.33
untrapped particle fractions	$\langle n_u \rangle/n_0, f_c$	0.55, 0.25
toroidal field strength	B_{t0}	2.1 T
vacuum RMP field magnitude	$\delta \hat{B}_{\rho m/n}^{\text{vac}}/B_{t0}$	3.3×10^{-4}
reference collisionality (ν_e/ω_u)	$\bar{R}q/\lambda_e$	0.017
relative electron pressure	$2\mu_0 n_e T_e/B_{t0}^2$	2.6×10^{-3}

- M. Murakami and X.Q. Xu, Phys. Plasmas **9**, 2037 (2002).
- ⁵H. Zohm, Plasma Phys. Control. Fusion **38**, 105 (1996).
- ⁶W. Suttrop, Plasma Phys. Control. Fusion **42**, A1 (2000).
- ⁷A. Loarte et al., “ITER ELM control requirements, ELM control schemes & required R & D,” paper ITR/1-4 at the 23rd International Atomic Energy Agency (IAEA) Fusion Energy Conference (FEC), 11–16 October 2010, Daejeon, Korea. Available at http://www-pub.iaea.org/MTCD/Meetings/cn180_papers.asp.
- ⁸R. Aymar, V.A. Chuyanov, M. Huguet, Y. Shimomura, ITER Joint Central Team and ITER Home Teams, Nucl. Fusion **41**, 1301 (2001).
- ⁹T.E. Evans, R.A. Moyer, P.R. Thomas, J.G. Watkins, T.H. Osborne, J.A. Boedo, E.J. Doyle, M.E. Fenstermacher, K.H. Finken, R.J. Groebner, M. Groth, J.H. Harris, R.J. La Haye, C.J. Lasnier, S. Masuzaki, N. Ohyabu, D.G. Pretty, T.L. Rhodes, H. Reimerdes, D.L. Rudakov, M.J. Schaffer, G. Wang, and L. Zeng, Phys. Rev. Lett. **92**, 235003 (2004).
- ¹⁰T.E. Evans, R.A. Moyer, K.H. Burrell, M.E. Fenstermacher, I. Joseph, A.W. Leonard, T.H. Osborne, G.D. Porter, M.J. Schaffer, P.B. Snyder, P.R. Thomas, J.G. Watkins and W.P. West, Nature Physics **2**, 419 (2006).
- ¹¹T.E. Evans, M.E. Fenstermacher, R.A. Moyer, T.H. Osborne, J.G. Watkins, P. Gohil, I. Joseph, M.J. Schaf-

- fer, L.R. Baylor, M. Bécoulet, J.A. Boedo, K.H. Burrell, J.S. deGrassie, K.H. Finken, T. Jernigan, M.W. Jakubowski, C.J. Lasnier, M. Lehnen, A.W. Leonard, J. Lonroth, E. Nardon, V. Parail, O. Schmitz, B. Unterberg and W.P. West, Nucl. Fusion **48**, 024002 (2008).
- ¹²O. Schmitz, T.E. Evans, M.E. Fenstermacher, E.A. Unterberg, M.E. Austin, B.D. Bray, N.H. Brooks, H. Frerichs, M. Groth, M.W. Jakubowski, C.J. Lasnier, M. Lehman, A.W. Leonard, S. Mordijck, R.A. Moyer, T.H. Osborne, D. Reiter, U. Samm, M.J. Schaffer, B. Unterberg, W.P. West, and the DIII-D and TEXTOR Research Teams, Phys. Rev. Lett. **103**, 165005 (2009).
- ¹³Y. Liu, A. Kirk, and E. Nardon, Phys. Plasmas **17**, 122502 (2010).
- ¹⁴M.S. Chu, L.L. Lao, M.J. Schaffer, T.E. Evans, E.J. Strait, Y.Q. Liu, M.J. Lanctot, H. Reimerdes, Y. Liu, T.A. Casper and Yuri Gribov, Nucl. Fusion **51**, 073036 (2011).
- ¹⁵N.M. Ferraro, Phys. Plasmas **19**, 056105 (2012).
- ¹⁶J.D. Callen, Phys. Rev. Lett. **39**, 1540 (1977).
- ¹⁷A.B. Rechester and M.N. Rosenbluth, Phys. Rev. Lett. **40**, 38 (1978).
- ¹⁸S.I. Braginskii, in *Reviews of Plasma Physics* edited by M.A. Leontovich (Consultants Bureau, New York, 1965), Vol. 1, p. 205.
- ¹⁹J.D. Callen, A.J. Cole, C.C. Hegna, S. Mordijck, R.A. Moyer, “RMP effect on pedestal structure and ELMs,” report UW-CPTC 11-13R, 19 March 2011 (to be published in Nuclear Fusion).
- ²⁰S. Mordijck, “Particle transport as a result of Resonant Magnetic Perturbations,” Ph.D. Thesis, University of California-San Diego, 2011.
- ²¹J.D. Callen, R.J. Groebner, T.H. Osborne, J.M. Canik, L.W. Owen, A.Y. Pankin, T. Rafiq, T.D. Rognlien and W.M. Stacey, Nucl. Fusion **50**, 064004 (2010).
- ²²R. Fitzpatrick, Phys. Plasmas **2**, 825 (1995).
- ²³C.C. Hegna and J.D. Callen, Phys. Fluids B **4**, 4072 (1992).
- ²⁴C.C. Hegna, Phys. Plasmas **6**, 3980 (1999).
- ²⁵J.D. Callen, A.J. Cole and C.C. Hegna, Phys. Plasmas **16**, 082504 (2009).
- ²⁶J.D. Callen, C.C. Hegna and A.J. Cole, Phys. Plasmas **17**, 056113 (2010).
- ²⁷S.P. Hirshman and D.J. Sigmar, Nucl. Fusion **21**, 1079 (1981).
- ²⁸C.T. Hsu, K.C. Shaing, R.P. Gormley and D.J. Sigmar, Phys. Fluids B **4**, 4023 (1992).
- ²⁹C. Bender and S. Orzag *Advanced Mathematical Methods for Scientists and Engineers* (Springer-Verlag, New York, 1999), p. 383 ff.
- ³⁰K.T. Tsang and J.D. Callen, Phys. Fluids **19**, 667 (1976).
- ³¹C.C. Hegna and J.D. Callen, Phys. Fluids B **5**, 104 (1993).
- ³²N.M. Ferraro, private communication, 2012.
- ³³Z. Chang and J.D. Callen, Nucl. Fusion **30**, 219 (1990).